Title

EQUILIBRIUM CONFIGURATIONS OF ROTATING CHARGED OR GRAVITATING LIQUID MASSES WITH SURFACE TENSION. PART II

Authors

Cohen, S.
Plasil, F.
Swiatecki, W.J.

Publication Date

1972-10-01

Submitted to Annals of Physics

LBL-1502
Preprint

EQUILIBRIUM CONFIGURATIONS OF ROTATING CHARGED OR GRAVITATING LIQUID MASSES WITH SURFACE TENSION. PART II.

S. Cohen, F. Plasil, and W. J. Swiatecki

October 18, 1972

Prepared for the U.S. Atomic Energy Commission under Contract W-7405-ENG-48

LBL-1502

DISCLAIMER

LBL-1502

EQUILIBRIUM CONFIGURATIONS OF ROTATING CHARGED OR GRAVITATING LIQUID MASSES WITH SURFACE TENSION. PART II.*

S. Cohen

Argonne National Laboratory
Argonne, Illinois 60440,

F. Plasil

Oak Ridge National Laboratory
Oak Ridge, Tennessee 37830,

and

W. J. Swiatecki

Lawrence Berkeley Laboratory
University of California
Berkeley, California 94720

October 18, 1972

* Reference 8 will be taken to be Part I in the present series of papers.

INTRODUCTION

This series of papers will present a survey of equilibrium configurations of rotating charged or gravitating liquid masses.

The theory of rotating homogeneous masses as idealized representations of planets, stars, and nebulae goes back to Newton's investigations on the figure of the earth. In the past two and a half centuries the theory has been developed by many illustrious mathematicians, among them Maclaurin, Jacobi, Riemann, Poincaré, Liapounoff, Jeans, Darwin, Cartan, Appell, and Lyttelton. In the last decade the subject was taken up anew by S. Chandrasekhar and N. Lebovitz and brought to a rare degree of perfection in Chandrasekhar's monumental work on "Ellipsoidal Figures of Equilibrium."[1]

The theory of a rotating liquid mass endowed with a surface tension but no gravitational forces was stimulated by Plateau's experiments 100 years ago with globes of oil suspended in a liquid of the same density. The experiments were discussed in connection with Laplace's nebular hypothesis of the origin of the solar system. An account of the earlier investigations is given in Appell's "Mécanique Rationnelle"[2] (Vol. 4, Ch. IX).

The theory of rotating liquid masses with a surface tension and a uniform electric charge arose in nuclear physics in connection with the study of nuclei endowed with large angular momenta. The major part of the binding energy of a nucleus is well represented by the model of a uniformly charged liquid drop with a surface tension, and the addition of a rotational energy to the conventional volume, surface, and electrostatic energies of the liquid drop model constitutes and interesting generalization.

A number of authors, among them Pik-Pichak,[3] Beringer and Knox,[4] Hiskes,[5] Sperber,[6] Carlson and Pau Lu,[7] Cohen, Plasil and Swiatecki,[8] Chandrasekhar,[9] Rosenkilde,[10] Mollenauer and Wheeler[11] have addressed themselves to this problem in the past 15 years.

It was pointed out in Refs. 7 and 8 that the nuclear problem of a rotating charged drop may be made to go over smoothly into the astronomical problem of an idealized rotating gravitating mass by imagining the electrostatic energy of the drop to be gradually decreased in magnitude, to go through zero, and to continue on to negative values, at which stage it becomes the energy of attractive Newtonian gravitation. In this way a continuous formal connection is established between the classic equilibrium configurations of idealized rotating astronomical masses, the flattened globes of Plateau, and the various equilibrium configurations of an idealized nucleus.

Thus a problem of irresistible scope presents itself: to discuss in a unified manner the equilibrium shapes of rotating masses representing at one extreme idealized atomic nuclei and at the other idealized heavenly bodies. The present series of papers is an attempt in this direction.

The study of stable and unstable configurations of equilibrium of a mechanical system, i.e., of the configurations where the potential energy is stationary with respect to all infinitesimal displacements, is a prerequisite to a full dynamical discussion of the system. This is rooted in the circumstance that ever since the rationalization of mechanics that is associated with the names of Lagrange and Hamilton, the theoretical description of any system may be formulated in a standard way. First the number and nature of the degrees of freedom of the system are defined,

after which a key function of these degrees of freedom, the Lagrangean or Hamiltonian is specified. One part of the Hamiltonian is the potential energy of the system, the other is its kinetic energy. The mapping out of the potential energy as a function of the degrees of freedom is a first step in understanding the properties of the system, and the location of the stationary points in these maps (minima, maxima, and saddle-point passes with various degrees of instability) is the first step in a survey of such maps. (We may remark parenthetically that this standard procedure has, in the main, survived the revolutionary replacement of classical mechanics by quantum mechanics. The writing down of a Lagrangean or Hamiltonian function and the mapping of a potential energy as a function of the degrees of freedom, is a step common to classical and quantal treatments of a problem; the distinction arises at the stage when the dynamical equations of motion are written down, classical in one case and quantal in the other.) The listing of the points where the potential energy is stationary in the many-dimensional configuration space provides a survey of the equilibrium shapes of the system. The nature of the stationary points (as given by the number of degrees of freedom with respect to which the energy is a minimum or a maximum) provides information regarding the stability or instability of the equilibrium shape in question.

In the case of static (nonrotating) systems the relation between the nature of the stationary points and the stability or instability of a system is simple and direct: a maximum in one or more degrees of freedom indicates instability. In the case of systems in uniform rotation (i.e. gyrostatic systems) the configuration of gyrostatic equilibrium may still be located by making stationary an effective potential energy (the

potential energy augmented by a centrifugal potential), but the relation between the nature of the stationary points (maxima, minima or saddles) and the stability or instability of the system is more subtle. The conventional view is that a maximum in one or more degrees of freedom indicates instability of motion in the presence of dissipative forces (secular instability) but not necessarily otherwise. (See, for example, Ref. 12, p. 15.) In any case the first step in a listing of the configurations for which the potential energy or effective potential energy is stationary, together with an indication of the number of degrees of freedom with respect to which the energy is a maximum. (We shall call this number the degree of secular instability of the configuration.)

II. FORMULATION OF THE PROBLEM

Consider a configuration of a rotating incompressible gravitating or uniformly charged fluid endowed with a surface tension, whose sharp boundary (which may or may not be simply-connected) is specified by a number of degrees of freedom (which may be infinite).

The effective potential energy, from which configurations of equilibrium may be deduced by differentiation, is given by

$$E = E_S + E_C + E_R , \tag{1}$$

where E_S is the surface energy, E_C the electrostatic or gravitational energy, and E_R is the rotational energy (Ref. 12, p. 26).

The surface energy E_S is equal to the surface area of the configuration in question, times the surface energy coefficient γ :

$$E_S = \gamma \oint d\sigma . \tag{2}$$

The quantity E_C is the sum of interactions between pairs of volume elements $d\tau_1$ and $d\tau_2$ interacting according to an inverse-distance potential:

$$E_C = (\text{constant}) \frac{1}{2} \iiint\!\!\iiint \frac{d\tau_1 \, d\tau_2}{r_{12}} . \tag{3}$$

The 'constant' is equal to the square of the (uniform) charge density in the electrostatic case, or to minus the square of the mass density, times the constant of gravitation, in the gravitational case.

The rotational energy will be taken as the square of the angular momentum L divided by twice the moment of inertia of the configuration in question

$$E_R = L^2/2\rho \iiint r_\perp^2 \, d\tau \, . \qquad (4)$$

Here $r_\perp$ is the perpendicular distance of the volume element $d\tau$ from the axis of rotation (passing through the center of mass of the system).

In Eq. (4) the moment of inertia is taken to be that of a rigid body. This is because the present paper will be confined strictly to configurations of gyrostatic equilibrium in which the only time-dependence of the motion of all fluid elements is a uniform rotation about a common axis with a common angular velocity. Other types of motion, where the boundary of the fluid rotates as a whole but fluid elements inside it execute nongyrostatic motions, are also of great interest (Ref. 1), but will be excluded from the present survey. This limitation is to a certain extent a natural one insofar as dissipative effects associated with relative motions of neighboring fluid elements (e.g. viscosity) tend to convert nongyrostatic to gyrostatic motions. Thus gyrostatic motions may be considered as governing the ultimate fate of a system after a sufficiently long lapse of time. One should bear in mind, however, that this time may in certain cases be very long, or even tend to infinity as the relevant dissipative effects tend to zero.*

Equations (1) - (4) describe the effective potential energy of the system and the problem to which we shall address ourselves is now defined: <u>to discuss the configurations of equilibrium given by the condition that $\delta E = 0$ for all infinitesimal variations of the degress of freedom specifying the system.</u>

Let us denote by $E_S^{(o)}$, $E_C^{(o)}$, $E_R^{(o)}$, and $E^{(o)}$ the surface, electrostatic (or gravitational), rotational and total energies of the spherical configuration. We may then write the deformation energy,

* Special caution should be exercised in this respect in the case of disconnected systems, e.g., Darwin's binary star system or the Roche problem of a satellite. In these cases the relevant dissipative effects may enter only through tidal couplings between the two bodies, and these may be very small. Nevertheless these small couplings may make all the difference between stability and secular instability, and their neglect has in some cases led to apparent contradictions regarding the stability of such configurations as inferred by different authors.

measured with respect to the energy of the sphere and expressed in units of the surface energy of the sphere, in the following dimensionless form, familiar in the literature of nuclear fission:

$$\xi = \frac{E - E^{(o)}}{E_S^{(o)}} = \frac{E_S - E_S^{(o)} + E_C - E_C^{(o)} + E_R - E_R^{(o)}}{E_S^{(o)}}$$

$$= (B_S - 1) + 2x(B_C - 1) + y(B_R - 1). \qquad (5)$$

Here B_S is the surface energy of the configuration in question, expressed in units of the surface energy of the sphere. It is a dimensionless function (strictly speaking a functional) of the shape of the drop, and assumes the value 1 for the spherical configuration. Similarly B_C and B_R are dimensionless functionals specifying the ratios of the electrostatic (gravitational) and rotational energies to their values for the sphere. Thus

$$B_S(\text{shape}) = E_S/E_S^{(o)},$$

$$B_C(\text{shape}) = E_C/E_C^{(o)},$$

$$B_R(\text{shape}) = E_R/E_R^{(o)},$$

where

$$E_S^{(0)} = 4\pi R^2 \gamma$$

$$E_C^{(0)} = \frac{3}{5}\frac{Q^2}{R} \quad \text{or} \quad -\frac{3}{5}\frac{M^2 G}{R} \tag{6}$$

$$E_R^{(0)} = \frac{L^2}{2\mathcal{I}_0} = \frac{1}{2}\cdot\frac{L^2}{\frac{2}{5}M R^2} .$$

In the above R is the radius of the spherical configuration, $\mathcal{I}_0$ its moment of inertia, γ is the surface tension coefficient (i.e., the surface energy per unit area), Q is the total charge on the drop, M its total mass, L its angular momentum and G is the constant of gravitation.

The two dimensionless parameters x and y in Eq. (5) specify the ratios of electrostatic (gravitational) and rotational energies of the sphere to the surface energy of the sphere:

$$x = \frac{E_C^{(0)}}{2E_S^{(0)}} = \frac{(\text{Charge})^2}{10\ (\text{Volume})\ (\text{Surface Tension Coefficient})} ,$$

$$\text{or} \quad \frac{-G\ (\text{Mass})^2}{10\ (\text{Volume})\ (\text{Surface Tension Coefficient})} ;$$

$$y = \frac{E_R^{(0)}}{E_S^{(0)}} = \frac{5}{16\pi}\ \frac{(\text{Angular Momentum})^2}{(\text{Mass})\ (\text{Radius})^4\ (\text{Surface Tension Coefficient})} . \tag{7}$$

The parameter y is a measure of (the square of) the angular momentum and thus of the size of the disruptive centrifugal forces compared to the cohesive surface tension forces. The parameter x is the conventional 'fissility parameter' of nuclear physics. For positive values of x it is a measure of the disruptive electrostatic forces and for negative values it is a measure of the cohesive gravitational forces, compared to the surface tension forces. We note that the surface energy of a spherical drop is equal to its gravitational energy when $x = -\frac{1}{2}$. For a liquid with the density and surface tension of water, for example, the radius of a spherical globe for which the two energies are equal is given by

$$R = (5\gamma / \tfrac{4}{3}\pi G\rho^2)^{1/3} = 10 \text{ meters, approximately.}$$

Thus the region of x values around minus one half would correspond to liquid globes (e.g. molten asteroids) with dimensions of this general order of magnitude.

If we wish to consider the conventional idealized astronomical problem of a gravitating fluid for which the surface energy is negligible, we have to take the limit where both $-x$ and y tend to infinity. It is then convenient to introduce the ratio of the rotational energy of a sphere to the magnitude of its gravitational energy, which ratio we shall denote by t

$$t = \frac{E_R^{(0)}}{-E_C^{(0)}} = \frac{y}{-2x} = \frac{25}{12}\,\frac{L^2}{G\,R\,M^3} .$$

The quantity ξ in Eq. (5) represents the deformation energy with respect to the energy of a rotating rigid sphere. It is sometimes more convenient to consider the deformation energy with respect to a nonrotating sphere; we write this as ζ, where

$$\zeta = \frac{E - E_S^{(0)} - E_C^{(0)}}{E_S^{(0)}} = (B_S - 1) + 2x(B_C - 1) + yB_R = \xi + y .$$

When the deformation energy is expressed in units of the gravitational energy, i.e., in units of $-E_C^{(0)}$ instead of $E_S^{(0)}$, we shall use in place of ζ the quantity η, defined as

$$\eta = \frac{E - E_S^{(0)} - E_C^{(0)}}{-E_C^{(0)}} = (-2x)^{-1}(B_S - 1) + (1 - B_C) + tB_R .$$

In the astronomical case this reduces to

$$\eta = (1 - B_C) + tB_R .$$

In the literature on the astronomical problem the amount of rotation in relation to the gravitational energy is usually described in one of three ways: by the dimensionless measure of the square of the angular velocity ω, namely

$\omega^2/2\pi G\rho$ (denoted by Appell by h), by the dimensionless measure of the kinetic energy, $\frac{1}{2}\mathcal{J}\omega^2$, namely $\frac{1}{2}\mathcal{J}\omega^2/(G M^2/R)$ (Lyttelton's T, Chandrasekhar's [T]), or by the dimensionless measure of the angular momentum $L/(G R M^3)^{1/2}$ (Chandrasekhar's [M], Lyttelton's H, Jeans' M, Darwin's μ). We note the relations

$$T = \frac{3}{10}(\mathcal{J}/\mathcal{J}_0)\, h ,$$

(where $\mathcal{J}/\mathcal{J}_0$ is the relevant moment of inertia of the figure in question in units of $\mathcal{J}_0$, the moment of inertia of a sphere) and, in particular,

$$t = \frac{25}{12}[M]^2 .$$

Thus our parameter t or $y/(-2x)$ is two and one-twelfth times the square of the conventional astronomical measure of angular momentum.

The specification of the two numbers x and y defines, through Eqs. (1 - 4), the energy characteristics of the system we are dealing with, and the equilibrium configurations may then be determined (if the functionals B_S, B_C, and B_R are known). If we imagine this done for a pair of values of x and y and we subsequently vary x and y, we generate <u>two-parameter families of equilibrium</u>

configurations. The case in which one parameter at a time is varied corresponds to the familiar situation of 'linear series of equilibrium configurations.' (See Refs. 2, 12.) The classic examples are the sequences of equilibrium shapes of rotating astronomical masses considered as functions of the amount of rotation. (Maclaurin spheroids, Jacobi ellipsoids, Poincaré pears, etc.) The systematic discussion of such families of equilibrium configurations and their stability leads to the notions of a 'point of bifurcation' (where two linear series cross when plotted as functions of the variable parameter) and to a 'limiting point' or 'turning point', where a family of equilibrium shapes doubles back on itself. These notions may be generalized to the present case where two parameters, x and y, are varied. A linear series of equilibrium shapes becomes a two-parameter 'sheet' of configurations. A crossing of two series becomes a crossing of two sheets along a 'bifurcation curve', and a limiting or turning point becomes a limiting or turning curve, where a sheet of solutions doubles back on itself. One of the advantages of ordering families of equilibrium configurations according to linear series or sheets is that formal connections may be established between different configurations that at first seem unrelated. A typical example is the case of a family of stable configurations and a family of saddle-point configurations between which a connection may be established. This may occur by way of a point or curve of bifurcation where the families cross and have a common member, or by way of a limiting point or limiting curve where one family is actually a smooth continuation of the other. We shall pay particular attention to the relations to one another of the various nuclear and astronomical families of equilibrium

configurations. We found considerable satisfaction in discovering continuous connections between, for example, the Poincaré-Liapounoff pears and the nuclear Businaro-Gallone asymmetric dumb-bells, or between the Bohr-Wheeler saddle-point shapes and Darwin's binary star system! Besides their entertainment value such connections can be useful in increasing one's understanding of the physical significance of various equilibrium shapes. Our study of the equilibrium configurations of rotating masses has been guided by the wish to establish all the relations in x-y space between the more important astronomical and nuclear families.

Owing to difficulties associated with the calculation of the electrostatic energy of nonaxially symmetric configurations we have succeeded only partially in making such a survey. In some cases we have been forced to compromise by introducing an approximation that treats certain shapes as axially symmetric when, in fact, they are not. Even though we believe our survey to be correct in its essential features, we are planning further calculations free of the above approximation. Since this may take some time we have decided to publish our work in a series of papers of which the first will describe principally results of immediate interest in applications to nuclear phsyics, where the imperfections of the present calculations have to be balanced against their practical relevance for current research.

III. SURVEY OF RESULTS

Our survey of equilibrium configurations will be made in terms of diagrams in x, y space: for any given x (a given charge or intensity of gravitation) we shall describe the sequence of equilibrium shapes as y (the amount of rotation) is increased. The range of x-values in these diagrams (Figs. 2a,b,c) is from -1 to $+1$. (The value $x = 1$ represents the maximum amount of charge that a droplet's surface tension can support. For $x > 1$ no stable undisintegrated configurations exist.) The range in y that we shall consider is from 0 to $+\infty$. For the sake of completeness we shall eventually consider families of equilibrium for $x < -1$, $x > 1$ and for $y < 0$. (The latter case corresponds to negative rotational energies--a negative centrifugal force!--and is of some interest.) In the present paper, however, the stress will be on nuclear applications, with x between 0 and 1, and $y \geq 0$.

(a) Stable Undisintegrated Configurations

For small amounts of rotation the originally spherical drop is flattened by the centrifugal force into an oblate spheroid, independently of the value of x, i.e., independently of whether we discuss a gravitating liquid mass with or without surface tension, or a charged nuclear droplet. For finite values of y the equilibrium configurations are no longer exact spheroids and we shall refer to these shapes as pseudospheroids or Hiskes shapes (Fig. 3). In the astronomical limit of zero surface tension the oblate shapes of equilibrium do happen to be exact spheroids: they are the Maclaurin spheroids. The spheroids or pseudospheroids continue to flatten with increasing rotation and they remain

stable until a certain critical value of y, denoted by y_I, which is a function of x. At this point the pseudospheroids become secularly unstable and a qualitative change takes place. The nature of the change depends on whether x is below or above a certain critical value x_c, which is today not yet determined exactly, but appears to be in the neighborhood of $x_c = 0.81$ (see last reference under (3)). This corresponds to heavy nuclei towards the end of the periodic table.

If $x > x_c$ the flat pseudospheroids become secularly unstable towards disintegration, by way of a triaxial deformation.

If $x < x_c$, and this includes the rest of the periodic table as well as uncharged droplets, molten asteroids and astronomical gravitating masses, the flat pseudospheroid becomes secularly unstable towards conversion into a nonaxially symmetric configuration of equilibrium, which branches off the pseudospheroids at the critical value y_I (see Figs. 2a,b,c). This new configuration has the symmetry of an ellipsoid with three unequal axes and rotates about its shortest axis. The other two axes are at first almost equal (when y exceeds the critical value by an infinitesimal amount and the equilibrium configuration is almost axially symmetric). Later these two axes become rapidly unequal, one of them becoming longer and longer as y increases, and the other tending to approximate equality with the shortest axis about which the rotation is taking place. The general appearance of these configurations is that of flattened cylinders with rounded ends and a somewhat elliptic cross section. In the astronomical limit of large negative x these configurations are exact ellipsoids (the Jacobi ellipsoids); otherwise the tips of the figure are more rounded. For certain values of x (in the

neighborhood of 0) there is even a suggestion of a dumb-bell or hourglass shape. We shall refer to these configurations as pseudo-ellipsoids, or as Beringer-Knox shapes.

As the angular momentum is increased beyond the first critical value y_I the pseudo-ellipsoids which exist for $x < x_c$ become more and more elongated under the influence of the centrifugal force until a second critical value of y is reached, denoted by y_{II}. At this value of y the family of triaxial pseudo-ellipsoids comes to an end by way of loss of equilibrium towards a reflection symmetric disintegration mode. If x is greater than a second critical value of x, denoted by x_{cc} (and equal to about -0.4), the pseudo-ellipsoids are stable shapes up to the critical value y_{II}, when they cease to exist. If, however, $x < x_{cc}$, the pseudo-ellipsoids lose stability against a reflection asymmetric disintegration mode along the dashed part of the critical curve denoted by y_{III} in Fig. 2. This occurs before the disappearance of the pseudo-ellipsoids at y_{II}, so that in the case of $x < x_{cc}$ the pseudo-ellipsoids exist but are unstable against asymmetry in the region between y_{III} and y_{II}.

We may summarize the situation as follows: A sufficient amount of rotation will always disintegrate a fluid mass, be it gravitating or charged. The critical amount of rotation is, naturally, a decreasing function of x, being given by the curve $y_I(x)$ for $0.81 < x < 1$, by $y_{II}(x)$ for $-0.4 < x < 0.81$ and by $y_{III}(x)$ for $-\infty < x < -0.4$.

The disintegration occurs by way of a <u>loss of stability</u> against a triaxial mode in the first case, by way of a <u>loss of equilibrium</u> against a reflection symmetric mode in the second case, and by way of <u>loss of stability</u> against a reflection asymmetric mode in the third case. Note

the distinction between loss of stability and loss of equilibrium. Loss of stability in a family of equilibrium shapes means that for a parameter (e.g. y) in excess of a critical value an equilibrium shape exists but has changed from stable to unstable, i.e., the second derivative of the energy has changed sign. Loss of equilibrium means that the family of equilibrium shapes has ceased to exist: with the parameter in excess of the critical value the condition for equilibrium, $\delta E = 0$, cannot be satisfied, i.e. the condition of the vanishing of the first derivative of the energy has no (real) solutions. As noted before, when we say "unstable" we mean "secularly unstable".

Finally a note about the astronomical limit $x = -\infty$, or $x^{-1} = 0$. The situation is similar to the case of $-\infty < x < x_{cc}$ in that increasing angular momentum leads to a loss of stability against a reflection asymmetric mode (at $t = 0.316$). Nevertheless the case of zero surface tension ($x^{-1} = 0$) is a special case, different from the case of a finite surface tension, however small, in that for $x^{-1} = 0$ the Jacobi ellipsoids are shapes of equilibrium for any value of y, even exceeding y_{II}. In this (astronomical) case y_{II} does not mark the end of the ellipsoids (a loss of equilibrium) but merely a loss of stability against a reflection symmetric disintegration mode. We reserve a detailed discussion of the subtle difference between a small surface tension and no surface tension for a future occasion.

(b) Saddle-Point Configurations

The stability of an undisintegrated configuration of equilibrium is ensured by the existence of a potential energy barrier and of an associated saddle-point shape (Fig. 1). In what follows we shall describe

the appearance of these saddle-point configurations, which are responsible for the stability of the undisintegrated configurations discussed in the preceding section, and which coincide with them at the moment when stability or equilibrium are lost along the critical curves y_I, y_{II} or y_{III}.

These equilibrium shapes are well known for a nonrotating charged drop, i.e., for $y = 0$. They resemble axially symmetric cylinders with rounded ends for x between about $2/3$ and 1 (tending to a sphere at 1), and symmetric dumb-bells or hourglass figures for x between about $2/3$ and zero (tending to two equal tangent spheres at $x = 0$). (See Ref. 13, p. 416.) On the other hand, when the amount of rotation is equal to the critical value for the disintegration of the liquid mass, the saddle-point shapes coincide with the undisintegrated shapes. The effect of rotation on the saddle-point shapes is a contraction of the cylinders and a filling up of the neck of the dumb-bells. The physical reason for this is that the unstable saddle-shapes must become more compact in order to be able to balance the centrifugal force.

Rotating saddle-point shapes are, in general, triaxial, and for $x \lesssim -0.4$ they are also asymmetric (pear-shaped). In practice, however, two of the three axes are usually approximately equal. They are, of course, exactly equal when the amount of rotation is zero, but even for larger amounts of rotation, up to the critical value y_{II} or y_{III}, they remain approximately equal provided only x is not too close to x_c (given by $x_c \approx 0.81$). For $x > 0.81$ the saddle shapes may have three substantially unequal axes, approximate axial symmetry about a direction perpendicular to the angular momentum for small y being replaced by axial symmetry about the angular momentum (at $y = y_I$).

But even for $x > x_c$ saddle shapes are substantially triaxial only when y is not too close either to $y = 0$ or $y = y_I$. We shall refer to the triaxial saddle shapes as the Pik-Pichak configurations.

(c) Disintegrated Configurations

On the far side of a saddle pass in the effective potential energy there exist one or more disintegrated configurations of equilibrium (see Fig. 1). The first problem here is to find, among the several such configurations, the one corresponding to an Absolute Minimum in the energy. We note that for any value of x, positive or negative, and for any y, a configuration of n equal spherical fragments at infinity, rotating infinitely slowly about the common center of mass, makes the effective potential energy stationary. Thus the moment of inertia of infinitely separated fragments is infinite and so the rotational energy is zero for any finite angular momentum. The interaction between the fragments is also zero and the fragments are thus in (neutral) equilibrium as regards changes in their separation coordinates.* If, moreover, the fragments

* The equilibrium is neutral in the sense that infinitesimal changes in the large (infinite) separations leave the energy unchanged. Finite changes--in fact changes sufficiently large to convert the large (infinite) separation into a finite separation--increase the energy if x is positive and decrease it if x is negative.

are all equal, the energy will, by symmetry, be stationary with respect to changes in their relative sizes.

Here we should point out that we take the notion of equilibrium in the strict formal sense of a condition wherein the (effective) potential energy E of Eq. (1) is stationary with respect to all degrees of freedom describing the configuration. In particular the degrees of freedom with respect to which we shall demand equilibrium always include the relative sizes of the fragments, even if the fragments are separated and there is no communication between them through a neck of matter. We regard the discussion of the physical transfer of matter from one fragment to another (whether in the case of fission fragments or stars) as a separate problem. It is beyond the scope of the present investigation, which is confined strictly to static aspects, i.e., to the formal mapping of the potential energy as a function of all the degrees of freedom, and the listing of configurations that make the energy stationary.

The energy of n equal fragments at infinity is given by the sum of surface and electrostatic (or gravitational) energies (see Refs. 13, 15):

$$\xi = (n^{1/3} - 1) + 2x(n^{-2/3} - 1) \tag{8}$$

or

$$\eta = \frac{1}{-2x}(n^{1/3} - 1) + (1 - n^{-2/3}) . \tag{8a}$$

The first term represents the surface energy: each of the n fragments has an area equal to $n^{-2/3}$ times the area of the original sphere, so, for n fragments, the total area, in units of the area of the standard sphere, is $n(n^{-2/3})$, or $n^{1/3}$. Similarly the second term represents the

electrostatic or gravitational self-energies, which scale as the inverse fifth power of the radius, i.e., as $n^{-5/3}$ for a single fragment, and which thus add up to $n(n^{-5/3})$ i.e., to $n^{-2/3}$ times the self-energy of the standard sphere.

The rotational energy does not appear in the above equations since it is zero for two or more fragments at infinity. It is important to note, however, that even for one 'fragment', i.e., for $n = 1$, the rotational energy may be made zero if an infinitesimal satellite, which does not sensibly modify the surface or electrostatic (gravitational) energies, is detached from the rotating mass and placed at infinity. Thus, if the relative orders of infinity in the distance and smallness of the satellite are chosen suitably, the moment of inertia of the whole configuration may be made infinite (despite the smallness of the satellite). The rotational energy is then zero for any finite angular momentum. This means that we may use Eqs. (8) and (8a), including the case $n = 1$, to select the Absolute Minimum in the effective potential energy for any value of x. By comparing ξ or η for different values of n we readily find that for $-\infty < x < 0.35121$ a single sphere (with an infinitesimal satellite at infinity) has the lowest energy, for $0.35121 < x < 0.61098$ two equal fragments at infinite separation have least energy, for $0.61098 < x < 0.86502$ three fragments, for $0.86502 < x < 1.11726$ four, etc. (see Ref. 15, p. 248).

It was pointed out in Ref. 14 that the ranges of x in which a given number of fragments represents an Absolute Minimum of the energy, are related to the tendency to form the most strongly bound fragments. In the case of nuclei, represented by the liquid drop model, the strongest binding occurs when $x = \frac{1}{4}$ (Ref. 14, p. 131). This corresponds to the

region of the periodic table in the vicinity of iron. Nuclei in this region are indeed among the relatively more abundant elements in nature. In the astronomical case the Absolute Minimum of energy is approached by a system consisting of a small satellite (or satellites) revolving at a large distance about a slowly rotating mass, the satellite(s) carrying most of the angular momentum. This is a situation somewhat reminiscent of the solar system or of the earth-moon system. It is an amusing thought that the same elementary considerations expressed by Eq. (8) or (8a), which suggest the relatively large abundance of medium weight elements in nature, should also suggest a relatively large abundance of very unequal binary or satellite systems in the domain of astronomy.

In addition to the disintegrated configurations of equilibrium consisting of n equal fragments at infinity (of which one, for any x, represents an Absolute Minimum) there are other disintegrated configurations of equilibrium possible. For example, if $x > \frac{1}{5}$, two unequal fragments at infinity may have a stationary energy if their relative sizes are adjusted suitably. (See Ref. 15, p. 256 and Ref. 14, Fig. 39.)

These configurations are sometimes of interest, and a general survey of many such configurations and of the relations between them will be given on a future occasion. For the present we return to the description of equilibrium shapes of more immediate practical interest, namely equilibrium shapes of idealized rotating nuclei: stable equilibrium shapes representing their ground states (deformed by the centrifugal force), and unstable saddle-point shapes associated with the barrier against disintegration.

IV. GRAPHS AND FIGURES

(a) Examples of Shapes

In Fig. 3 we show a series of meridian sections of axially symmetric shapes of equilibrium for $x = 0$ and y ranging from 0 to 2.25. For $y < 0.2829$ these figures are ground state equilibrium shapes, but for $y > 0.2829$ they are all secularly unstable with respect to triaxial deformations for which the equator of the figure becomes elliptic and the figure acquires three unequal axes.

Figures 4 - 9 illustrate ground states and saddle shapes for various values of x and y.

Figure 4a refers to $x = 0$, $y = 0$. There is no rotation and so the ground state is a sphere and the saddle shape is the configuration of two tangent spheres (Ref. 13). As the rotation is increased to $y = 0.28$ (Fig. 4b) the sphere is seen to flatten into an axially symmetric (Hiskes) shape. (At this y-value it is about to lose stability against a triaxial deformation.) The saddle shape (Pik-Pichak shape) has become an hourglass figure with a thin neck. The true hourglass figure has a somewhat elliptic cross section; the one illustrated in Fig. 4b was obtained from a calculation in which the cross section was restricted to be circular. The curve in Fig. 4b represents therefore a mean longitudinal section of the hourglass figure. The same will be true of other triaxial shapes in the following figures.

In Fig. 4c the rotation has been increased to $y = 0.64$. The ground state shape is now a triaxial (Beringer-Knox) shape, whose mean longitudinal section is the less indented of the two shapes in Fig. 4c. The other curve is the mean longitudinal section of the Pik-Pichak saddle shape.

Figures 5a-d show a similar sequence for $x = 0.3$. For $y = 0$ and $y = 0.16$ the ground state is an axially symmetric Hiskes shape, for $y = 0.24$ and $y = 0.4$ it is a triaxial Beringer-Knox shape, whose mean section is shown. We may note that for $x = 0.3$ the value $y = 0.4$ is quite close to the critical value y_{II} where the fission barrier vanishes ($y_{II} = 0.42$) and as a result the Beringer-Knox ground state and the Pik-Pichak saddle are quite close in appearance. (At $y = y_{II}$ they coalesce.)

Figures 6a,b,c show a similar sequence for $x = 0.6$, Figs. 7a,b do this for $x = 0.7$, and Figs. 8a,b refer to $x = 0.8$. A very small amount rotation is now sufficient to cause disintegration.

Figure 9a shows a set of x,y values chosen to be very close to the critical line y_{II}. The solid line is the mean longitudinal section of the Beringer-Knox shape and the dashed line gives an indication of the mode of deformation with respect to which loss of equilibrium occurs at the critical point y_{II}. (A necking-in and elongation of the figure.)

Figure 9b shows the same thing for $x = 0.5$, $y = 0.18$.

(b) Principal Axes and Moments of Inertia

Plots of the equilibrium shapes for all pairs of x and y values of interest would take up an inordinate amount of space. In Figs. 10 and 11 we attempt to give the most important features of these shapes (the principal axes and the principal moments of inertia) in the form of graphs with x as the abscissa and y as labels on the curves.

In Fig. 10 consider for example the family of curves labeled with the number 0.16. These curves give, as functions of x, the axes (in units of R) of the ground and saddle shapes of drops rotating with a y-value of 0.16. Thus the curve CD gives the minor axis and the curve

AB gives the two (equal) major axes of the oblate, axially symmetric Hiskes pseudospheroid corresponding to the stable ground state equilibrium configuration. Figure 10 shows that at an x-value of about 0.356, at the circled points, a pair of new curves branches off at B, and a new curve starts at D. The former two curves (BG and BF) give the major and median axes, and the latter curve (DF) gives the minor axis of the Beringer-Knox pseudo-ellipsoid which, for $x > 0.356$, is the stable rotating ground state. At a value of x near 0.523 the family of triaxial stable shapes comes to an end. The major axis bends back at G and the median and minor axes bend back at F. Beyond the bend (i.e. at values of x decreasing below 0.523) these curves give now the major, median and minor axes of the rotating Pik-Pichak saddle-point shape for $y = 0.16$. Thus the whole set of curves with the label 0.16 enables one to estimate the three axes R_{max}, R_{med}, R_{min} of the axially symmetric oblate shape, of the triaxial ground state (when it exists) and of the triaxial saddle-point shape. As an illustration let us read off the $y = 0.16$ curves at $x = 0.4$. We find that for the oblate pseudospheroid:

$$R_{max} = R_{med} = 1.118R\,, \qquad R_{min} = 0.775R\,;$$

for the triaxial ground state:

$$R_{max} \approx 1.35R, \quad R_{med} \approx 0.91R, \qquad R_{min} \approx 0.74R;$$

and for the triaxial saddle shape:

$$R_{max} \approx 2.1R, \quad R_{med} \approx R_{min} \approx 0.31R.$$

(For the more elongated saddle shapes the two lesser axes are close in magnitude and only a single curve is used to indicate their mean value.)

The axes of the various equilibrium shapes may be similarly estimated for other values of x and y. For $x \gtrsim 0.81$ the situation is somewhat different in that the triaxial ground state pseudo-ellipsoids do not exist. (For practical purposes they may be disregarded already for $x \gtrsim 0.7$.) For example the set of curves labeled 0.01 gives the axes of the ground state spheroids (attaining values of $R_{max}/R = 1.04$ and $R_{min}/R = 0.92$ at $x = 0.9$ --the circled points) and of the saddle shape whose major and median axes branch off the circled point at I and whose minor axis joins the circled point at J.

As y tends to zero the major axis becomes the down-sloping curve labeled 0.0 and the median and minor axes coalesce and become the upward-sloping curve labeled 0.0. These curves correspond to the major and minor axes of nonrotating saddle-point shapes. (Compare Ref. 13, Fig. 2.) The axes of the rotating oblate ground-state pseudospheroids tend, in the limit $y \to 0$, to the horizontal line $R/R = 1.0$ corresponding to a sphere.

The principal moments of inertia of the rotating equilibrium shapes may be estimated from Fig.11 in a similar manner. Taking again the set of curves labeled 0.16 as an example, a vertical line at $x = 0.4$ cuts this set at $\mathcal{I}/\mathcal{I}_0 = 0.51,\ 0.75,\ 0.945,\ 1.265,\ 1.33,\ 1.46$ and 4.26. These numbers correspond to the following estimates:

For the oblate pseudospheroids

$$\mathcal{I}_{max} = \mathcal{I}_{med} = 1.265\,\mathcal{I}_0, \qquad \mathcal{I}_{min} = 0.945\,\mathcal{I}_0;$$

for the triaxial ground state:

$$\mathcal{I}_{max} \approx 1.46\,\mathcal{I}_0, \qquad \mathcal{I}_{med} \approx 1.33\,\mathcal{I}_0, \qquad \mathcal{I}_{min} \approx 0.75\,\mathcal{I}_0;$$

for the triaxial saddle shape:

$$\mathcal{I}_{max} \approx 4.26\mathcal{I}_0, \qquad \mathcal{I}_{med} \approx \mathcal{I}_{min} \approx 0.51\mathcal{I}_0 .$$

In the above $\mathcal{I}_0$ is the moment of inertia of a rigid sphere. Note that $\mathcal{I}_{max}$ is the moment of inertia taken about the shortest axis (about which the rotation is taking place), $\mathcal{I}_{med}$ the moment about the median axis and $\mathcal{I}_{min}$ the moment about the longest axis. Again, for elongated saddle shapes, only one mean value is shown for the approximately equal quantities $\mathcal{I}_{max}$ and $\mathcal{I}_{med}$.

(c) Energies

The energies of the ground states and saddle shapes described above may be deduced from Figs. 12a,b,c and 13a,b. Figure 12a shows the energies (in unites of $E_S^{(0)}$) of the rotating shapes, as functions of x and for different values of y. For each value of y the energy is given with respect to the energy of the rigid sphere rotating with the same angular momentum. The more nearly horizontal curves give the energies of the oblate Hiskes shapes, the more steeply diving curves which start at the circled points refer to the Beringer-Knox shapes, and the very steep curves joining the latter in a sharp cusp are the energies of the Pik-Pichak saddle shapes. Let us once again use the case of $y = 0.16$ as an example. For $x = 0$ Fig. 12a gives for its energy $\xi = -0.0131$, which means that the energy of an uncharged rotating sphere with surface tension $E_S^{(0)}$ (and with an initial rotational energy $E_R^{(0)} = 0.16\, E_S^{(0)}$) goes down by $0.0131E_S^{(0)}$ when the sphere is allowed to deform into its equilibrium Hiskes shape. If the sphere is charged (i.e. if the x-value is finite) this energy relief increases as shown by the trend of the

curve labeled 0.16 in Fig. 12a. (This is because the stiffness of the drop against deformations is softened by the electric charge.)

At the circled point (for $x = 0.358$) the Hiskes configuration becomes secularly unstable with respect to conversion into a triaxial Beringer-Knox shape, whose energy is lower and rapidly decreases further with increasing x. Even so the energy of the Pik-Pichak saddle point decreases even faster with x (the almost linear steep curve) and the energy difference between the two curves (which is the fission barrier) vanishes at $x = 0.528$. At this point their common energy is given by $\xi = -0.0367$, i.e. it is $0.0367\ E_S^{(0)}$ units below the energy of a rotating rigid sphere.

As usual, for $x \gtrsim 0.81$, the Beringer-Knox shapes are absent and the vanishing of the barrier against fission occurs directly by the osculation of the Pik-Pichak and Hiskes curves at the circled points.

Figure 12b is similar to 12a but covers a larger range of y-values. Figure 12c gives an expanded view of the high x range.

Figures 13a,b give the energy differences between the ground state (a Hiskes or Beringer-Knox shape, whichever is lower) and the Pik-Pichak saddle. Thus they give directly the height of the fission barrier (in units of $E_S^{(0)}$) in its dependence on x and y. They may also be used to deduce the energy of the Pik-Pichak shapes (for which Figs. 12a,b,c are generally inadequate) by adding the barrier to the ground state, i.e.,

$$\xi_{\text{Pik-Pichak}} = \xi_{\text{Ground}} + \xi_{\text{Barrier}} .$$

In Fig. 13a the circled points connected by a short-dashed line indicate where the ground state changes from a Hiskes to a Beringer-Knox shape

(Hiskes shape above the line, Beringer-Knox below). The long-dashed line indicates that to the left of it the Pik-Pichak saddles are unstable against deviations from reflection symmetry. (Caution should then be exercised in interpreting the energy difference between the reflection symmetric Pik-Pichak shape and the ground state as a fission barrier--see Ref. 13, p. 416). Figure 13b gives an expanded view of the high x end of the range.

One comment should be made about the expected accuracy of the graphs in Figs. 10 to 13. For the axially symmetric Hiskes shapes all results are essentially exact; on the other hand for the triaxial shapes there are substantial inaccuracies, especially in the plots of the axes and moments of inertia. Without going into the details of the approximations underlying the calculations of the triaxial figures we may say that we consider the graphs as adequate semi-quantitative guides for the discussion of those shapes, but that calculations of their properties with controlled and high accuracy is still a project for the future on which we hope to report at a later date.

V. APPLICATIONS TO NUCLEI

In this section we shall illustrate some applications to nuclear problems--especially heavy ion physics--of the results described above. The applications will deal with practical estimates of critical angular momenta, the stability against fission of rotating nuclei and some estimates of limits to compound nucleus formation in heavy ion collisions. The possibility of producing highly deformed triaxial nuclear shapes will be mentioned. For definiteness of the discussion we shall use the case of Ag^{107} bombarded with Ne^{20} ions as an illustration of the use of the graphs.

(a) Units and Critical Values

Since all energies are given in units of $E_S^{(0)}$, the surface energy of the spherical drop, the first step is to calculate this quantity. We use the formula for the nuclear surface energy from Ref. 16, according to which

$$E_S^{(0)} = 4\pi R^2 \gamma = c_2 A^{2/3},$$

where

$$c_2 = 17.9439\,(1 - \kappa I^2)\ \text{MeV}$$

$$\kappa = 1.7826.$$

Here I is the relative neutron excess, i.e. $I = (N - Z)/A$, where N, Z, A are the neutron, proton and mass numbers of the nucleus.

For the case of the compound nucleus La^{127}, corresponding to an amalgamation of Ne^{20} and Ag^{107}, this gives $E_S^{(0)} = 444.89$ MeV. Similarly the Coulomb energy expression necessary for the calculation of the fissility parameter x, is given by Ref. 16 as

$$E_C = 0.7053 \frac{Z^2}{A^{1/3}} \text{ MeV} = 455.89 \text{ MeV} .$$

Note that this is not the Coulomb energy of La^{127} estimated according to Ref. 16, but what the Coulomb would be if the charge distribution were sharp rather than diffuse. It is this quantity which is relevant for the definition of x (see Ref. 17, p. 58) and thus

$$x = \frac{E_C^{(0)}}{2E_S^{(0)}} = \frac{1}{50.883(1 - 1.7826\, I^2)} \cdot \frac{Z^2}{A}$$

$$= 0.5124 \quad \text{for} \quad La^{127}.$$

In order to calculate the y-value for a given nucleus with angular momentum L $(=\hbar\ell)$ we use the following formula for $E_R^{(0)}$

$$E_R^{(0)} = \frac{1}{2} \frac{\hbar^2 \ell^2}{\frac{2}{5} MR^2} = \frac{5}{4} \cdot \frac{\hbar^2}{M_0 r_0^2} \cdot \frac{\ell^2}{A^{5/3}} .$$

The mass M of the nucleus was written as $M_0 A$ and its radius as $r_0 A^{1/3}$, where M_0 is a nominal mean nucleon mass and r_0 a nominal radius constant. We took for M_0 the average between the mass of a neutron and the mass of a hydrogen atom ($M_0 = 939.15$ MeV). For r_0 we took 1.2249 F, the value that goes with the Coulomb energy coefficient of 0.7053 MeV in the mass formula of Ref. 16. (Since the purpose of this section is to illustrate the use of the graphs and formulae and not to discuss the most realistic way of estimating nuclear sizes and moments of inertia, we do not attempt any refinements on such nominal values of nuclear parameters.)

Thus we find

$$E_R^{(0)} = 34.540 \frac{\ell^2}{A^{5/3}} \text{ MeV},$$

and

$$y = \frac{5}{4} \frac{\hbar^2}{M_0 r_0^2 c_2} \frac{\ell^2}{A^{7/3}}$$

$$= \frac{1.9249}{(1 - 1.7826I^2)} \frac{\ell^2}{A^{7/3}} . \qquad (9)$$

(As very rough, easily remembered formulae, we have

$$x \approx \frac{1}{50} \frac{Z^2}{A}$$

$$y \approx 2 \frac{\ell^2}{A^{7/3}} .)$$

For any nucleus specified by A, Z and ℓ we are now in a position to calculate x and y and thus use the earlier figures described. For example, from Fig. 2b we deduce that for La^{127} (with $x = 0.5124$) the two critical values of y are $y_I = 0.1112$ and $y_{II} = 0.175$. In the case of y_I the following formulae may be used:

$$y_I = 0.2829 - 0.3475x - 0.0016x^2 + 0.0501x^3$$

for $0 \leq x \leq 0.75$ and

$$y_I = \frac{7}{5}(1 - x)^2 - 4.5660(1 - x)^3 + 6.7443(1 - x)^4 ,$$

for $0.75 \leq x \leq 1.0$.

These formulae have the correct behavior at $x = 0$ and for $x \to 1$, represent the graphical values satisfactorily and are joined smoothly at $x = 0.75$. From the equation relating y and ℓ^2 (Eq. (9)) we deduce that

the critical angular momenta ℓ_I and ℓ_{II} corresponding to y_I and y_{II} are $\ell_I = 67.79$ and $\ell_{II} = 85.05$. Thus up to an angular momentum corresponding to about 68 units of $\hbar$ an idealized drop representing La^{127} would have an axially symmetric oblate equilibrium shape, whereas between about 68 and 85 units the predicted equilibrium shape has three unequal axes.

(b) Energies

The way in which the barrier against fission, B_f, goes down with increasing angular momentum may be deduced from Fig. 13. For example at the critical value y_I ($\ell_I = 67.79$) we find from Fig. 13a that $\xi = 0.0175$ and consequently $B_f = (0.0175)(444.89) = 7.79$ MeV. This may be contrasted with the value $\xi = 0.090$, $B_f = 40.0$ MeV for the case of zero angular momentum ($y = 0$). The ground state energy of La^{127} with the critical angular momentum ℓ_I may be deduced from Fig. 12a. Thus at $x = 0.5124$ we estimate ξ to be -0.0116 (the ground state is on the verge of changing from a Hiskes to a Beringer-Knox shape, and is thus on a curve that may be imagined as joining the circled points in Fig. 12a). Hence the ground state energy is $(-0.0116)(444.89) = -5.16$ MeV. The energy of the Pik-Pichak saddle point is then deduced as $\xi_{PP} = -0.0116 + 0.0175 = 0.0059$, which converts to 2.62 MeV. These energies are all with respect to a rotating rigid sphere with the same angular momentum. This energy is $E_R^{(0)}$, equal to $E_S^{(0)}y$, which in the case considered is thus $(444.89)(0.1112) = 49.47$ MeV. Hence with respect to the energy of a nonrotating sphere (i.e. with respect to what is a commonly used baseline--the energy of a spherical liquid drop taken from Ref. 16) we deduce the following energy values:

Energy of nonrotating sphere	0 MeV
Energy of nonrotating saddle	40.0 MeV
Energy of rotating rigid sphere	49.47MeV
Energy of rotating ground state	44.31MeV
Energy of rotating saddle	52.10MeV.

(c) Cross Sections

In a two-body collision there is a simple proportionality between the angular momentum $L(=\hbar\ell)$ and the impact parameter b of the colliding bodies (the perpendicular distance between the initial direction of the center of mass of the projectile and the center of mass of the target). The area πb^2 of the "impact circle" is the cross section for processes with angular momenta less than the angular momentum associated with b. As a result it is possible to translate our calculations regarding angular momenta (for example the critical angular momenta ℓ_I and ℓ_{II}) into statements about cross sections.

The relation between the angular momentum L and the impact parameter b in a collision between two masses M_{TARGET} and $M_{PROJECTILE}$ is

$$L = b\sqrt{2E_{CM}\,M_{red}}$$

or

$$b^2 = \frac{L^2}{2\,M_{red}} \cdot \frac{1}{E_{CM}} = \frac{\hbar^2}{2M_0} \cdot \frac{A}{A_T\,A_P} \cdot \frac{\ell^2}{E_{CM}}$$

$$= 20.7293\ \frac{A}{A_T\,A_P}\ \frac{\ell^2}{E_{CM}/\mathrm{MeV}}\ (\mathrm{fermi})^2$$

or

$$\pi b^2 = 651.23\ \frac{A}{A_T\,A_P}\ \frac{\ell^2}{E_{CM}/\mathrm{MeV}}\ \mathrm{mb}.$$

Here E_{CM} is the center of mass energy, M_{red} is the reduced mass

$M_T M_P/(M_T + M_P)$, A_T and A_P are the mass numbers of the target and projectile and A is their sum. If we wish to write b^2 in terms of y rather than ℓ^2 we recall that the definition of y is:

$$y = \frac{E_{rot}^{(0)}}{E_S^{(0)}} = \frac{1}{2} \frac{L^2}{\frac{2}{5} MR^2} \frac{1}{E_S^{(0)}} .$$

Elimination of L^2 between this expression and that for b^2 gives a relation between b^2 and y which may be written as

$$\pi b^2 = \pi R^2 \frac{2}{5} \frac{A^2}{A_T A_P} \cdot \frac{y}{E_{CM}/E_S^{(0)}} . \qquad (10)$$

$$= 338.32 \, (1 - 1.7826I^2) A^{10/3} y / A_T A_P E_{CM} \text{ millibarns,}$$

with E_{CM} in MeV. For a given angular momentum (a given y) this may be considered as a relation between the cross section πb^2 and the center of mass bombarding energy E_{CM}. Using again the case of $Ne^{20} + Ag^{107} = La^{127}$ as an example we find the numerical relation

$$\pi b^2 = 38.65 \frac{\ell^2}{E_{CM}/\text{MeV}} \text{ millibarns.}$$

Taking this time for ℓ the critical value ℓ_{II} associated with the vanishing of the fission barrier ($\ell_{II} = 85.05$) we get $\pi b_{II}^2 = 279552/E_{CM}$ mb, where E_{CM} is in MeV. This curve is the curve labeled $B_f = 0$ in Fig. 14. It divides the πb^2 vs E_{CM} plane into two regions: above this curve the angular momentum of the colliding system is too large to be supported by the nucleus La^{127}. Below this curve the rotating nucleus La^{127} would still have a finite fission barrier.

We may use our graphs to calculate the locus in πb^2 vs E_{CM} space corresponding to any given value of the fission barrier. Let us take for example the case $B_f = 11$ MeV (the reason for this choice will appear presently). In units of $E_S^{(0)}$ this corresponds to $\xi = 11/(444.89) = 0.02472$. Using Fig. 13a we estimate that at $x = 0.5124$ a rotation corresponding to $y = 0.0983$ would have this ξ-value. This value of y corresponds to $\ell = 63.74$ (Eq. 9) and hence the corresponding πb^2 is given by:

$$\pi b^2 = 157030/E_{CM} \text{ mb} \qquad \text{(from Eq. 10).}$$

This is the curve marked $B_f = 11$ in Fig. 14.

It is instructive to plot in the same figure an estimated contact cross-section curve, i.e. the impact parameter (or its square times π) at which, for a given energy, the two nuclei come into contact. From conservation of energy and momentum it readily follows that the minimum distance of approach r_m in the collision of two bodies starting with impact parameter b and center-of-mass energy E_{CM} is related to the potential $V(r)$ acting between them by

$$\left(\frac{b}{r_m}\right)^2 = 1 - \frac{V(r_m)}{E_{CM}} .$$

When the minimum distance of approach is of the order of the sum of the radii of the two nuclei contact takes place in the sense that nuclear forces begin to come into play. More precisely we may set r_m for contact to be the sum of the radii $R_1 + R_2$, augmented by a distance d, which allows for the diffuseness of the nuclear surfaces and the finite range of nuclear forces. This quantity is expected to be of the order of a couple of fermis and approximately the same for all pairs of nuclei.

We may thus write for the cross section for contact

$$\pi b_c^2 = \pi(R_1 + R_2 + d)^2\left(1 - \frac{V_c}{E_{CM}}\right),$$

where

$$V_c = V(R_1 + R_2 + d) \approx \frac{Z_1 Z_2 e^2}{R_1 + R_2 + d} = \frac{1.4400\ Z_1 Z_2}{R_1 + R_2 + d}\ \text{MeV},$$

where $R_1 + R_2 + d$ is in fermis. In the last expression we have inserted as an estimate of the interaction energy at contact the electrostatic energy of two spherical nuclei. (We do not consider refinements to this estimate arising from nuclear deformations or the contribution of nuclear forces at contact.)

In Fig. 14 we show two contact cross-section curves based on the above formula with $d = 2$F and $d = 1.5$ F, respectively. Such choices of d, when used in conjunction with a radius parameter r_0 equal to 1.2249 F, reproduce in a fair manner experimental contact cross sections and contact energies. (Related to what are usually called "reaction cross sections" and "Coulomb barriers".) Choices of d below the range $1\frac{1}{2}$ - 2 F would correspond to progressively harder contact between the nuclei, in which more than just the extreme fringes of the nuclear densities and force fields come into play.

The significance of the plot in Fig. 14 is as follows (see also Refs. 8 and 18). In the area marked X , a compound nucleus is not possible since there is no potential energy barrier to prevent an immediate re-disintegration of the system. In the area Y + Z such a barrier is present--a potential energy hollow exists in the configuration space of the system. In this case a compound nucleus may or may not be formed depending on the dynamics of the collision after the moment of tangency.

Depending on many factors the dynamics may be such that the system misses the potential energy hollow altogether, or that it passes through it without being captured, or that it is captured. We would like to suggest the name "composite nucleus" for the state of the composite system consisting of the more or less amalgamated target and projectile, tracing out a dynamical path in configuration space between the moment of contact and either capture into the compound nucleus state or re-disintegration. The expression "compound nucleus" should be reserved for the description of the system after capture in the potential energy hollow. The expression "composite nucleus" then takes care of a system that may well correspond to an intimate contact or even transient amalgamation of target and projectile but without capture into a compound system (either because the system misses the hollow or passes through it, or because the hollow isn't there at all).

In cases where a hollow exists (i.e. below the curve labeled $B_f = 0$ in Fig. 14) and a compound nucleus is formed, there is still the question whether it will decay by particle emission (emission of neutrons, protons, alpha particles etc.) or by fission into comparable parts. Which of the two is more likely to happen depends on the relative sizes of the barriers for particle emission and fission. The curve labeled $B_f = 11$ in Fig. 14 shows the locus where the fission barrier is 11 MeV, which for the La^{127} nucleus in question is about the value of the neutron binding energy. (Emission of neutrons is often--but by no means always--the dominant mode of particle decay.) The $B_f = 11$ curve is thus expected to be, roughly, the dividing line between decay by fission (above the curve) and by particle emission (below). We expect then that even if a

compound nucleus is formed in a given collision between Ne^{20} and Ag^{107}, it would not survive during the de-excitation process if the conditions of the collision correspond to points above a curve roughly like the curve BC in Fig. 14. The degree to which the expectations based on Fig. 14 are borne out experimentally is discussed in Ref. 19. In particular a curve like ABC does seem to account for the formation and survival of the compound system in the reactions $Ne^{20} + Ag^{107}$ and $O^{16} + Al^{27}$.

On the other hand a recent article by Zebelman and Miller (Ref. 20) appears to give clear evidence that in other reactions a lower limiting angular momentum than that given by a curve such as ABC in Fig. 14 sets a bound on the formation and survival of a compound system. Thus in three reactions ($B^{11} + Tb^{159}$, $C^{12} + Gd^{158}$, $O^{16} + Sm^{154}$) designed to lead to the same compound nucleus Yb^{170} (and the same exitation energy for a given angular momentum), the experimental cross sections for formation and survival of the compound nucleus fall below the prediction based on a curve like ABC. The deviation becomes progressively more pronounced for the reactions induced by the lighter ions. A possible explanation may be that for a light ion to bring in the same angular momentum as a heavy one it must in general be traveling faster and/or at a larger impact parameter. This, coupled with the fact that the cohesion (i.e. the total binding energy as well as the barrier against disintegration) of a light ion is smaller, leads to the expectation that in many cases it may be too much to ask of a light ion to bring in a large angular momentum: the ion is traveling too fast and/or too nearly in a peripheral trajectory to amalgamate with the target. In such

collisions the light projectile will often disintegrate, its outer parts being sheared off. Thus, for a range of impact parameters below even a solid contact curve, and in some cases even below a curve like BC in Fig. 14, a compound nucleus may not be formed because of unfavorable initial conditions at the moment of tangency. In such cases even though a deep hollow exists in the potential energy surface in configuration space the initial conditions are such that the system is not given a chance to be captured in the hollow to form a compound nucleus.

(d) A Limiting Nuclear Angular Momentum

An interesting prediction of our calculations is that no nucleus can support more than a limiting angular momentum of about 100 units of $\hbar$. Figure 15 shows what happens when the plot from Fig. 2 of the critical value $y_{II}(x)$ (where the fission barrier vanishes) is converted into a plot of ℓ_{II} by means of Eq. (9). The plot is against the mass number A for nuclei taken along Green's smooth approximation to the valley of beta stability:

$$N - Z = \frac{0.4\, A^2}{200 + A} .$$

We see that neither light nor heavy nuclei can support many units of angular momentum (the former simply because of their small size, the latter because of their reduced stability caused by the Coulomb energy). The nuclei able to support the highest angular momenta occur near $A \approx 130$ in Fig. 15, but even in that case 97 units of $\hbar$ will make their fission barriers vanish.

The dashed curve in Fig. 15 shows the angular momentum required to lower the fission barrier of a nucleus to 8 MeV (a figure taken as

representative of the neutron binding energy of nuclei along the valley of beta stability). This curve gives an indication of the maximum amount of angular momentum that a compound nucleus could support and still survive the risk of fission in the de-excitation process (by getting rid of its excitation energy through particle emission). The maximum angular momentum in this case is about 77 units for $A \approx 140$.

(e) Super-Deformed Nuclei

Our calculations predict that for angular momenta greater than a critical amount corresponding to y_I the stable equilibrium shape becomes a triaxial configuration, with often a rather large deformation. For example, for a nucleus with a fissility parameter x equal to 0.45 and y equal to 0.16, Fig. 10 predicts an equilibrium shape with $R_{max} \approx 1.52\ R$, $R_{med} \approx R_{min} \approx 0.75\ R$, i.e. a ratio of axes of about 2:1. From Fig. 11 the moment of inertia about the axis of rotation is about 1.7 times the moment of inertia of a rigid sphere. Nuclei with such extreme deformations would be interesting objects to study experimentally if they could be produced. Of the several conditions that have to be satisfied to make such a study feasible the first is that one should be able to form (and ensure the survival of) a compound system with an angular momentum in excess of ℓ_I. Figure 15 shows that there exists a range of light and medium beta-stable nuclei up to $A \approx 145$ where fission barriers in excess of 8 MeV are expected even with angular momenta greater than ℓ_I. Figure 16 shows the calculated fission barriers for nuclei along Green's valley of beta stability and with angular momenta just equal to the critical value ℓ_I. It is seen that for very light or for heavy nuclei the fission barrier is likely to be less than the

neutron binding energy, and the cross sections for the survival of such nuclei would be small. On the other hand, for an optimum choice of the system, in the region of medium weight nuclei with $A \approx 66$, fission barriers as high as 18 MeV are expected at the angular momentum just sufficient to produce triaxial shapes. However, in order to produce a triaxial shape with a considerable elongation, of the order of a 2:1 ratio of axes, an angular momentum in excess of the critical value ℓ_I would be required, and the fission barrier would decrease below the curve displayed in Fig. 16.

We shall illustrate the above considerations by five reactions aimed to form compound systems with masses in the range from $A = 105$ down to $A = 24$ and ratios of axes of about 2:1.

1. $Ne_{10}^{20} + Rb_{37}^{85} = Ag_{47}^{105}$

Using our graphs and formulae we find for Ag^{105} the following parameters:

$x = 0.4217$, $y_I = 0.1398$, $\ell_I = 60.86$, $y_{II} = 0.275$, $\ell_{II} = 85.36$.

If as an example we pick a y-value equal to 0.16 (i.e. $\ell = 65.11$) the three axes of the rotating nucleus are $R_{max}/R \approx 1.42$, $R_{med}/R \approx 0.85$, $R_{min}/R \approx 0.72$. The moment of inertia about the axis of rotation is $\mathcal{I}_{max}/\mathcal{I}_0 \approx 1.58$ and the fission barrier is $B_f = 9.20$ MeV. The binding energies of the first two neutrons that might be emitted from Ag^{105} are estimated as $B_n(105) = 10.86$ MeV, $B_n(104) = 9.04$ MeV. (In estimating these binding energies we use the Lysekil mass formula[16] without shell effects and without corrections for the rotation of the Ag

nucleus). The least center-of-mass bombarding energy needed to produce nuclear reactions with an angular momentum $\ell = 65.11$ is given by $E_{CM}^{(min)}$ where

$$E_{CM}^{(min)} - V_c = 20.7293\ \ell^2\ \frac{A}{A_T A_P}\ \frac{1}{(R_1 + R_2 + d)^2}\ .$$

Using $d = 1.5$ F we find $V_c = 52.18$ MeV, $E_{CM}^{(min)} = 104.24$ MeV. If we take a bombarding energy 10 MeV higher than this minimum, i.e. $E_{CM} = 114.24$ MeV ($E_{LAB} = 141.12$ MeV) we find for the internal excitation energy of the rotating Ag^{105} nucleus with $\ell = 65.11$ the following result:

$$E_x = W + E_{CM} - E_S^{(0)}(y + \xi_{Gr}) = 57.39 \text{ MeV}.$$

In the above equation W (-2.42 MeV) is the mass difference between the sum of the masses of target and projectile and the mass of the non-rotating Ag^{105} (the latter as given by the Liquid Drop part of the Lysekil mass formula), and $E_S^{(0)}(y + \xi_{Gr})$ is the rotational and deformation energy of the rotating equilibrium configuration, whose dimensionless energy ξ_{Gr} is read off as -0.021 from Fig. 12b. The excitation energy of 57.39 MeV could be dissipated for example by the emission of four or five neutrons. A nucleus which managed to survive fission in this de-excitation process would still have an angular momentum close to $\ell = 65.11$ and a mass number only a little less than $A = 105$. Its energy with respect to the nonrotating liquid drop ground state would be approximately $E_S^{(0)}(y + \xi_{Gr})$ which is 54.43 MeV in our case. An energy of about this magnitude and an angular momentum of about 65.11 units would

have to be released in a cascade of electromagnetic transitions.

2. $Ar_{18}^{40} + Cu_{29}^{65} = Ag_{47}^{105}$

The same compound nucleus Ag^{105} with $\ell = 65.11$ might be formed using Ar^{40} ions, the advantage being a lower excitation energy in the compound system. Thus we find $V_c = 70.82$ MeV, $E_{CM}^{(min)} = 102.32$ MeV. Again taking a center mass energy 10 MeV higher, i.e. $E_{CM} = 112.32$ MeV ($L_{LAB} = 181.44$ MeV), we find $E_x = 42.36$ MeV. ($W = -14.52$ MeV in this case.) Thus 3 or 4 neutrons could carry away this excitation. All the other estimates are as before.

3. $O_8^{18} + Ti_{22}^{48} = Zn_{30}^{66}$

Here $x = 0.2720$, $y_I = 0.1893$, $\ell_I = 41.30$, $y_{II} = 0.453$, $\ell_{II} = 63.89$. Taking $y = 0.24$ we find $\ell = 46.50$, $R_{max}/R \approx 1.51$, $R_{med}/R \approx 0.83$, $R_{min}/R \approx 0.70$, $\varphi_{max}/\varphi_0 \approx 1.71$, $B_f = 10.83$ MeV, $B_n(66) = 11.26$ MeV, $B_n(65) = 9.05$ MeV, $V_c = 27.66$ MeV, $W = 20.31$ MeV. The minimum energy to produce reactions with $\ell = 46.50$ is $E_{CM}^{(min)} = 68.46$ MeV. Using $E_{CM} = 78.46$ we find $E_x = 40.38$ MeV, which would require the emission of about 3 neutrons. The energy to be released by gamma rays would be about 58.38 MeV.

4. $O_8^{16} + Al_{13}^{27} = Sc_{21}^{43}$

Here $x = 0.2017$, $y_I = 0.2132$, $\ell_I = 26.77$, $y_{II} = 0.538$, $\ell_{II} = 42.53$. Taking $y = 0.28$ we find $\ell = 30.68$, $R_{max}/R \approx 1.54$, $R_{med}/R \approx 0.81$, $R_{min}/R \approx 0.68$, $\varphi_{max}/\varphi_0 \approx 1.73$, $B_f = 9.46$ MeV, $B_n(43) = 13.75$ MeV, $B_n(42) = 11.22$ MeV, $V_c = 18.13$ MeV, $W = 16.05$ MeV.

The minimum energy to produce reactions with $\ell = 30.68$ is $E_{CM}^{(min)} = 46.59$ MeV. Using $E_{CM} = 56.59$ ($E_{LAB} = 90.12$ MeV) we find $E_x = 21.37$ MeV. After de-excitation the nuclei surviving fission would have to emit about 51.27 MeV in gamma rays.

The above is one of the few reactions for which there is experimental evidence that a compound system with an angular momentum close to or even in excess of ℓ_I was formed and survived fission. Thus in Ref. 21 it is estimated that at a bombarding energy of 105 MeV nuclei with angular momenta up to about 35 units are formed and survive.

5. $C_6^{12} + C_6^{12} = Mg_{12}^{24}$

Here $x = 0.1179$, $y_I = 0.2420$, $\ell_I = 14.45$, $y_{II} = 0.640$, $\ell_{II} = 23.50$. Taking $y = 0.32$ we find $\ell = 16.62$, $R_{max}/R \approx 1.56$, $R_{med}/R \approx 0.82$, $R_{min}/R \approx 0.68$, $\mathcal{J}/\mathcal{J}_0 \approx 1.76$, $B_f = 7.82$ MeV, $B_n(24) = 14.48$ MeV, $V_c = 7.29$ MeV, $E_{CM}^{(min)} = 26.18$ MeV. Using $E_{CM} = 36.18$ MeV ($E_{LAB} = 72.36$ MeV) we find $E_x = 8.65$ MeV. Such an excitation is below the neutron emission threshold and de-excitation would have to proceed by gamma emission (or fission). Nuclei that survived fission would still have an energy of 39.71 MeV to be emitted as electromagnetic radiation.

To summarize, the above estimates suggest that it should be possible to form super-deformed nuclei for a range of projectile and target combinations. Compound nuclei with masses in the range of about 40 to 100 should easily survive the risk of fission when the angular momentum is only just sufficient to produce triaxial shapes. For angular momenta necessary to produce shapes with a ratio of axes of about 2:1

it seems that in general the fission barrier is reduced to about the neutron binding energy. Loss of cross section due to fission is then to be expected, though it need not be catastrophic, and could be reduced somewhat by working with neutron-rich projectiles and targets (which would lead to compound nuclei with lower neutron binding energies).

The outstanding problem is to devise methods that would identify the presence of such super-deformed nuclei which in some existing experiments[21] may already have been produced without being detected. These methods would presumably be based on the analysis of the electromagnetic radiations emitted by such systems, but we shall not go into these questions here.

ACKNOWLEDGMENTS

We would like to thank J. A. Wheeler and J. Mollenauer for correspondence and discussions describing their calculations on rotating ellipsoids. We have benefited from discussions with B. C. Carlson and C. E. Rosenkilde and especially from several exchanges of views with S. Chandrasekhar regarding problems of stability. The assistance of Jean Reece and Joan Phillips in drawing up tables and graphs was much appreciated.

REFERENCES

1. S. Chandrasekhar, "Ellipsoidal Figures of Equilibrium," Yale University Press, 1969.

2. P. Appell, "Traité de Mécanique Rationnelle," Gauthier-Villars, Paris, 1932, Vol. 4.

3. G. A. Pik-Pichak, J. Exptl. Theoret. Phys. (U.S.S.R.) 34, 341 (1958), translated in Soviet Physics JETP 34, 238 (1958); J. Exptl. Theor. Phys. (U.S.S.R.) 42, 1294 (1962), translated in Soviet Physics JETP 15, 897 (1962); J. Exptl. Theor. Phys. (U.S.S.R.) 43, 1701 (1962), translated in Soviet Physics JETP 16, 1201 (1963).

4. R. Beringer and W. J. Knox, Phys. Rev. 121, 1195 (1961).

5. J. R. Hiskes, "The Liquid Drop Model of Fission Equilibrium Configurations and Energetics of Uniformly Rotating Charged Drops," University of California Lawrence Radiation Laboratory Report UCRL-9275 (1960).

6. D. Sperber, Phys. Rev. 130, 468 (1963).

7. B. C. Carlson and Pao Lu, Proceedings Rutherford Jubilee International Conference, Manchester, 1961, J. B. Birks, Ed. (Heywood and Co., London, 1962), p. 291.

8. S. Cohen, F. Plasil and W. J. Swiatecki, Proceedings Third Conference on Reactions Between Complex Nuclei, edited by A. Ghiorso, R. M. Diamond and H. E. Conzett, University of California Press, 1963, p. 325; University of California Radiation Laboratory preprint UCRL-10775, 1963.

9. S. Chandrasekhar, Proc. Roy Soc. (London) A286, 1 (1964).

10. C. E. Rosenkilde, J. Math. Phys. 8, 98 (1967).

11. J. Mollenauer and J. A. Wheeler, private communications, 1962 and 1965.

12. R. A. Lyttelton, "The Stability of Rotating Liquid Masses," Cambridge University Press, Cambridge, England, 1958.

13. S. Cohen and W. J. Swiatecki, Ann. Phys. (N. Y.) 22, 406 (1963).

14. S. Cohen and W. J. Swiatecki, Ann. Phys. (N. Y.) 19, 67 (1962).

15. W. J. Swiatecki, Proceedings Second International Conference on Peaceful Uses of Atomic Energy, Geneva, 1958, Pergamon Press, London, Paper P/651, USA.

16. W. D. Myers and W. J. Swiatecki, Arkiv för Fysik, 36, 343 (1967).

17. W. D. Myers and W. J. Swiatecki, Nucl. Phys. 81, 1 (1966).

18. W. J. Swiatecki, "Common Features and Differences Between Fission and Heavy Ion Physics," talk presented at European Conference on Nuclear Physics, Aix-en-Provence, France, June 26-July 1, 1972, to appear in Comptes-Rendus; Lawrence Berkeley Laboratory preprint LBL-972, June 1972.

19. M. Blann and F. Plasil, Phys. Rev. Letters 29, 303 (1972).

20. A. M. Zebelman and J. M. Miller, "On the Role of Angular Momentum in Complete Fusion Reactions," Preprint, October 1972.

21. L. Kowalski, J. C. Jodogne, and J. M. Miller, Phys. Rev. 169, 894 (1968).

FIGURE CAPTIONS

Fig. 1. Sketch of a two-dimensional potential energy surface illustrating different types of equilibrium points. The hollow A is a metastable minimum, separated from the Absolute Minimum C by a saddle-point B, with one degree of instability. The mountain top D has two degrees of instability.

Fig. 2a. Various critical rotational parameters y in their dependence on the fissility parameter x. Triaxial shapes appear between y_I and y_{II}. Saddle shapes are stable against reflection asymmetric distortions to the right of the dot-dashed portion of y_{III}. Triaxial shapes are unstable against asymmetry between the dashed portion of y_{III} and y_{II}. The critical curves y_{IV} and y_V will be discussed in future installments of this series of papers.

Fig. 2b. A portion of Fig. 2a on an enlarged scale.

Fig. 2c. A portion of Fig. 2b on an enlarged sclae.

Fig. 3. Meridian sections of rotating equilibrium shapes for $x = 0$ and y between 0 and 2.25.

Fig. 4. Ground states (heavier lines) and saddle shapes (lighter lines) for $x = 0$ and various values of y. In all figures H refers to "Hiskes", BK to "Beringer-Knox" and PP to "Pik-Pichak". Hiskes shapes have axial symmetry about the axis of rotation (vertical axis). The Beringer-Knox and Pik-Pichak shapes shown have approximate symmetry about the horizontal axis and only a mean transverse section is displayed for these shapes. (For $x = 0$, $y = 0$ the saddle shape is two spheres in contact.)

Fig. 5. Similar to Fig. 4 but for $x = 0.3$.

Fig. 6. Similar to Fig. 4 but for $x = 0.6$.

Fig. 7. Similar to Fig. 4 but for $x = 0.7$

Fig. 8. Similar to Fig. 4 but for $x = 0.8$.

Fig. 9. Two Beringer-Knox ground state shapes on the verge of loosing equilibrium against a symmetric division mode, indicated by the dashed line. Only mean transverse sections of the somewhat triaxial shapes are shown.

Fig. 10. The principal axes of families of equilibrium figures as functions of the fissility parameter x, for different values of the rotation parameter y (given as labels on the curves). See text for an explanation of the plot.

Fig. 11. The principal moments of inertia (in units of $\mathcal{I}_0$, the moment of inertia of a rigid sphere) plotted against x. The labels refer to the rotational parameter y. The moments of inertia about the axis of rotation are always greater than 1. See text for an explanation of the plot.

Fig. 12a. Ground state and saddle-point energies (with respect to the energy of a rotating rigid sphere, and in units of its surface energy $E_S^{(0)}$) plotted against the fissility parameter x for different values of the rotation parameter y. The most nearly horizontal curves refer to Hiskes shapes, the steeper curves to the right of the circled points to Beringer-Knox shapes, and the very steep curves to Pik-Pichak shapes.

Fig. 12b. Similar to 12a but for a different range of x and y values. For $y \geq 0.28$ the ground states shown are all Beringer-Knox shapes.

Fig. 12c. Similar to 12a but for x values close to 1. The ground states are all Hiskes shapes, joined at the circled points by Pik-Pichak shapes.

Fig. 13a. The difference between the energy of the Pik-Pichak saddles and the ground states (in units of the surface energy of the sphere) plotted versus x for different values of y. To the right of the long-dashed curve the Pik-Pichak saddles are stable against reflection asymmetric distortions and the curves are then barriers for symmetric fission. The ground states are Hiskes shapes above the short-dashed curve and Beringer-Knox shapes below. Fission barriers are obtained from these plots.

Fig. 13b. Similar to 13a but for x close to 1.

Fig. 14. A "collision diagram" of the square of the impact parameter b (times π) versus the center-of-mass energy E_{CM}, for the bombardment of Ag^{107} by Ne^{20}. The diagram shows a division into distant and close collisions, with a band of intermediate collision in between. The line labeled $B_f = 0$ shows where the fission barrier of a compound nucleus would vanish and the line $B_f = 11$ where it would be 11 MeV. Under certain assumptions the curve ABC would give approximately the cross section for the formation and survival of the compound nucleus.

Fig. 15. The curve ℓ_{II} is the angular momentum at which the fission barrier of a beta-stable nucleus with mass number A is predicted to vanish. In the range of angular momenta between ℓ_I and ℓ_{II} the ground state is predicted to be a triaxial Beringer-Knox shape. Below the dashed curve the fission barriers for the rotating beta-stable nuclei considered are highter than 8 MeV.

Fig. 16. A plot of the fission barrier in MeV for nuclei along the valley of stability with angular momenta just sufficient to produce triaxial Beringer-Knox ground states.

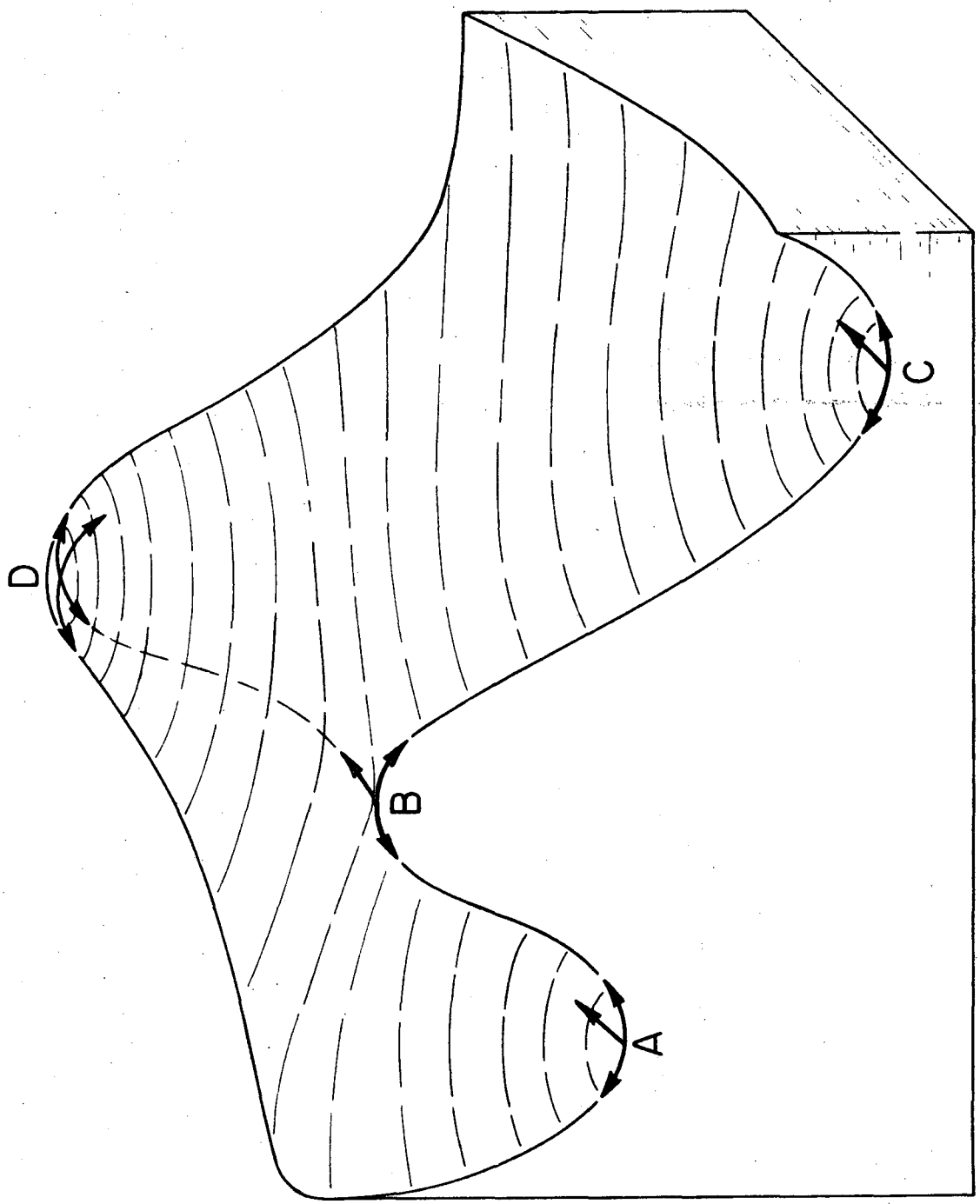

XBL7210-4360

Fig. 1

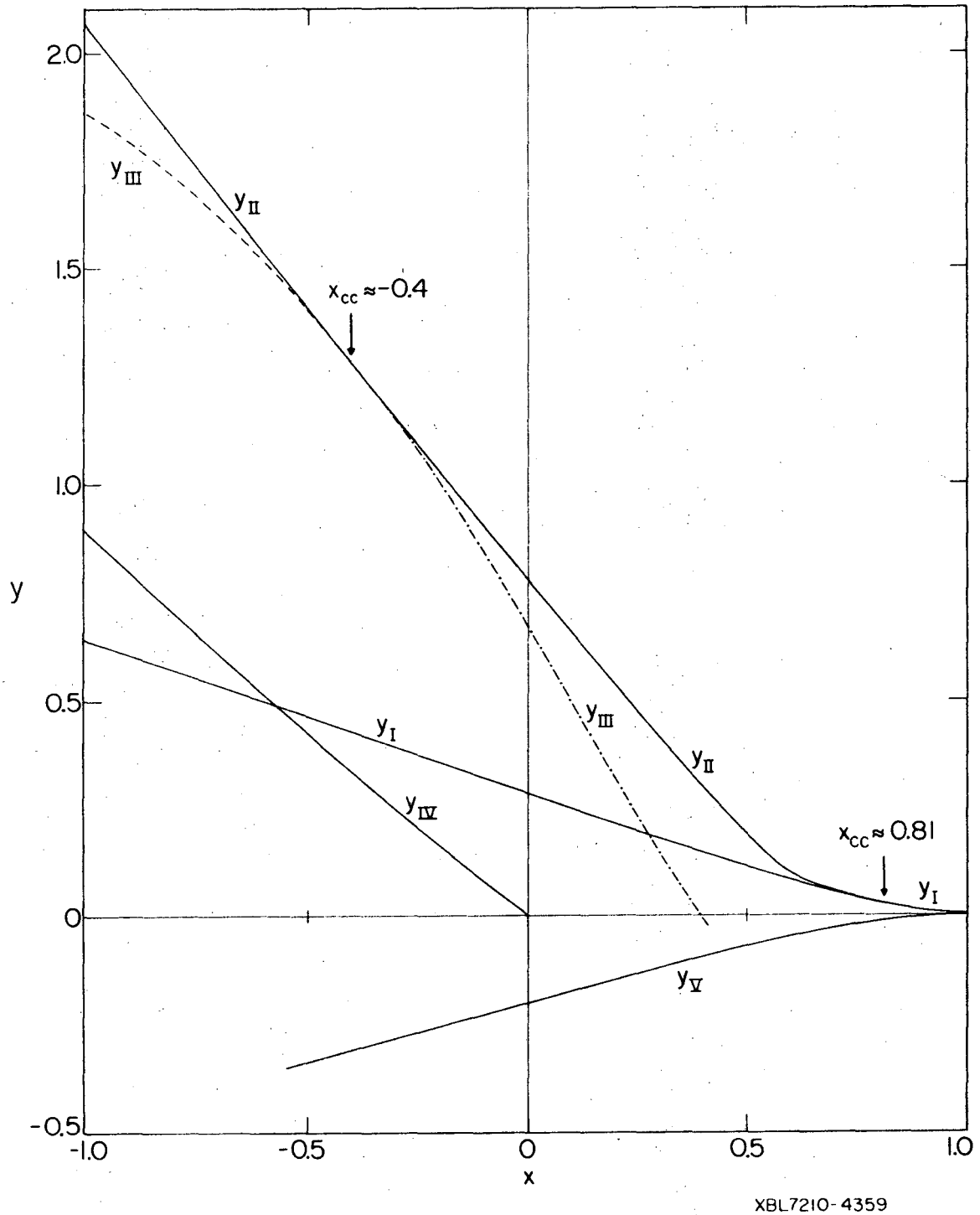
2.0
1.5
1.0
0.5
0
-0.5
y
-1.0
-0.5
0
0.5
1.0
x
y_{III}
y_{II}
$x_{cc} \approx -0.4$
y_I
y_{IV}
y_{III}
y_{II}
$x_{cc} \approx 0.81$
y_I
y_V
XBL7210-4359

Fig. 2a

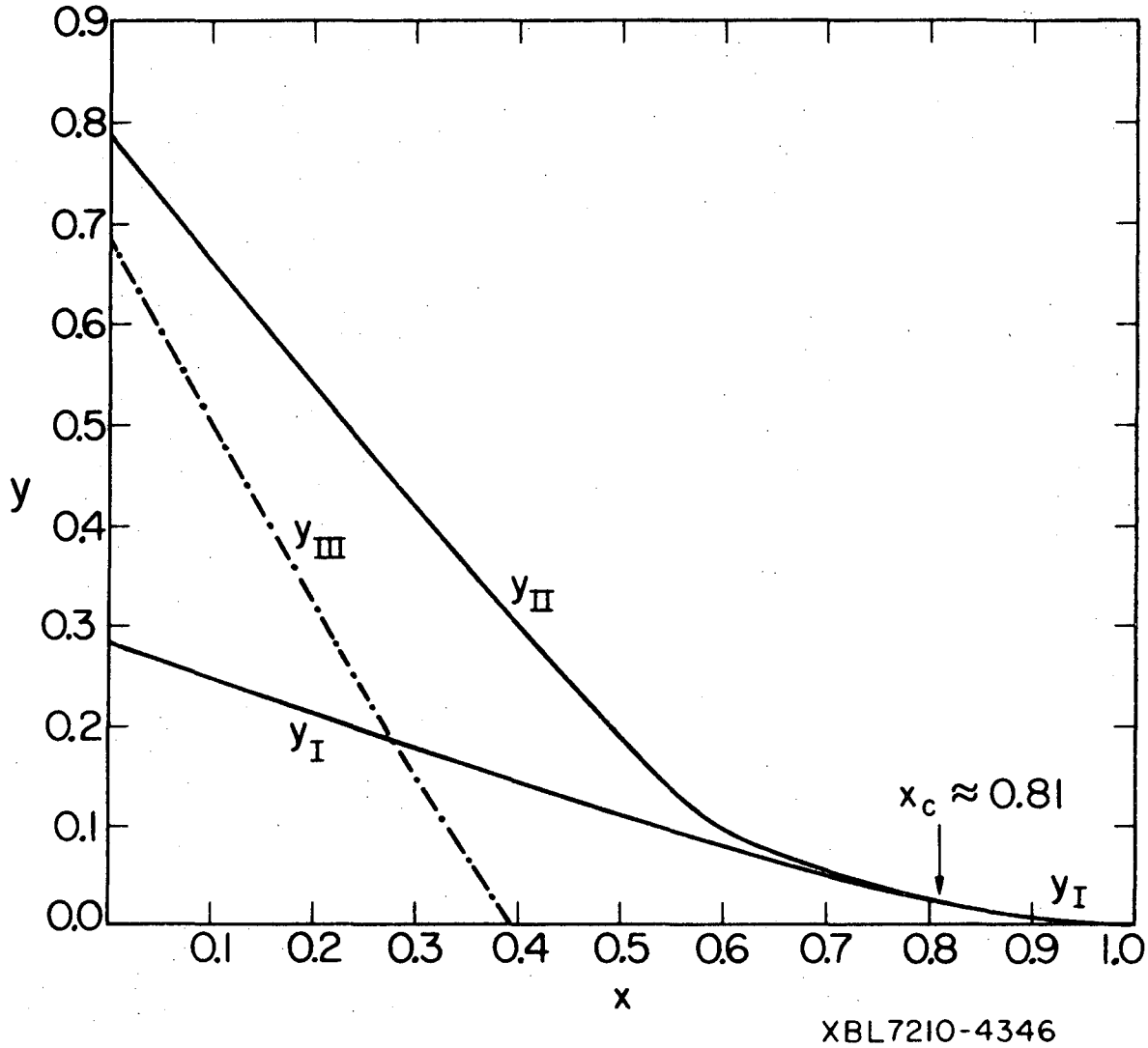

Fig. 2b

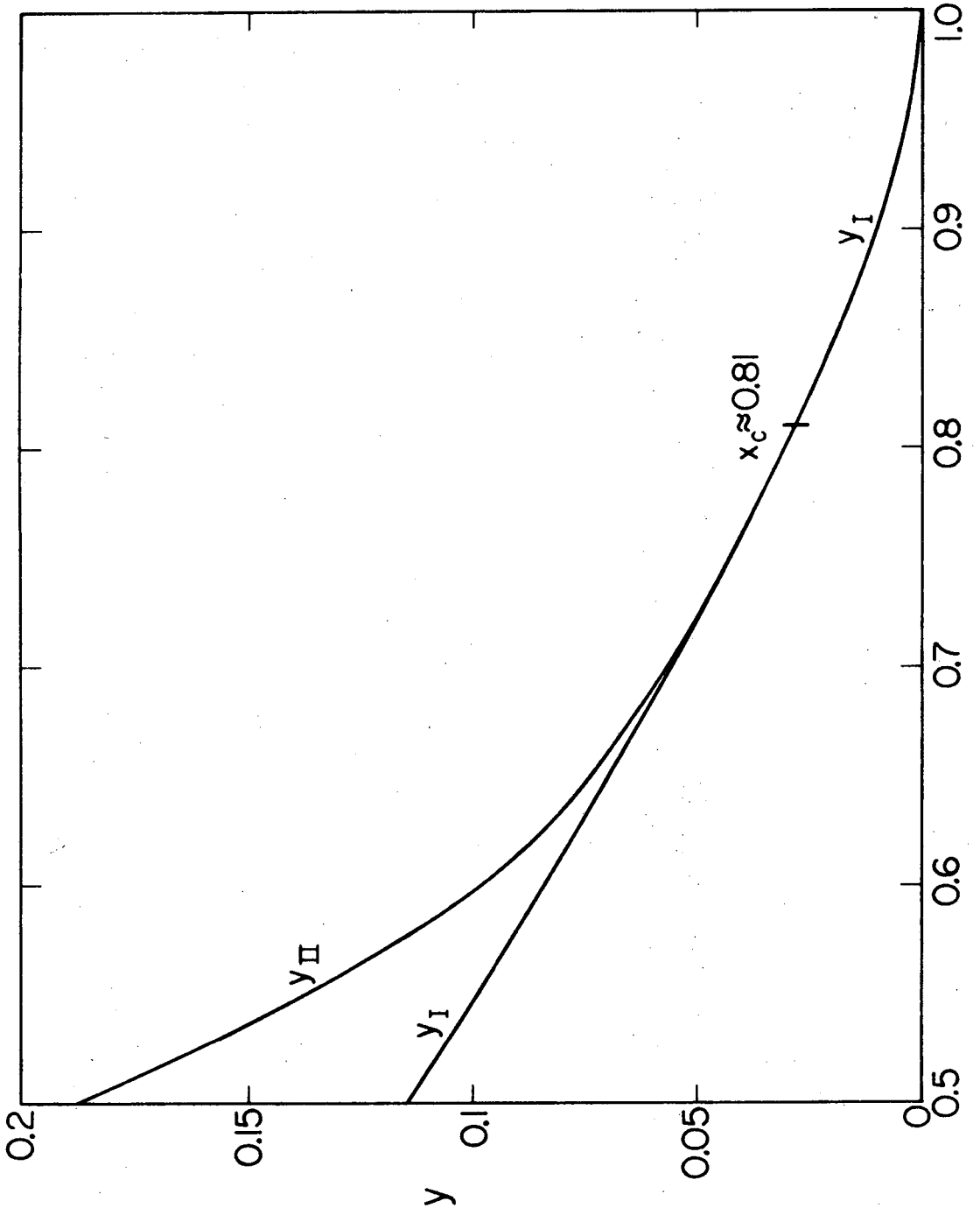

XBL7210-4347

Fig. 2c

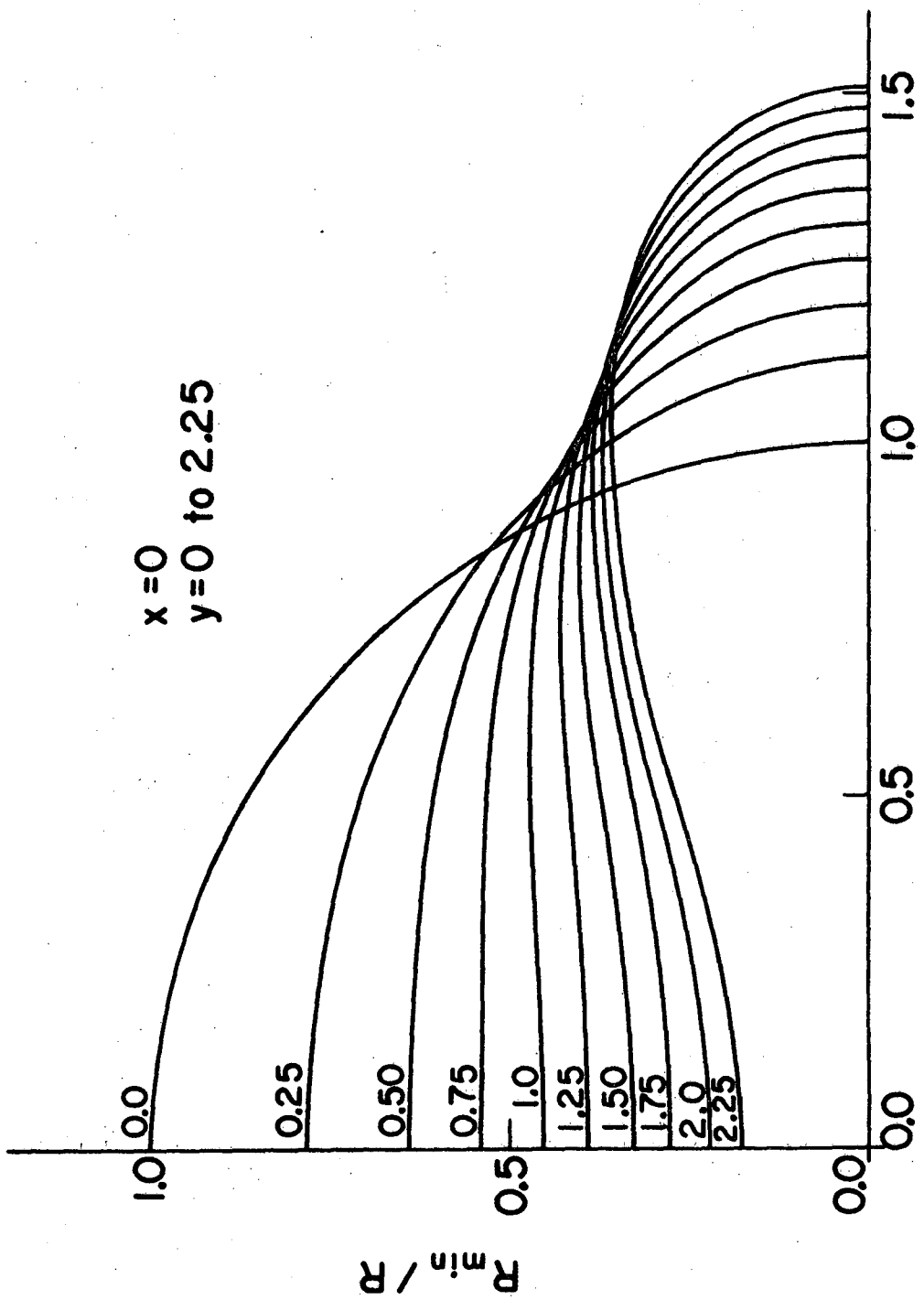
x=0
y=0 to 2.25
0.0
0.25
0.50
0.75
1.0
1.25
1.50
1.75
2.0
2.25
1.0
0.5
0.0
R_{min}/R
0.0
0.5
1.0
1.5
R_{max}/R
XBL 7210-4354

Fig. 3

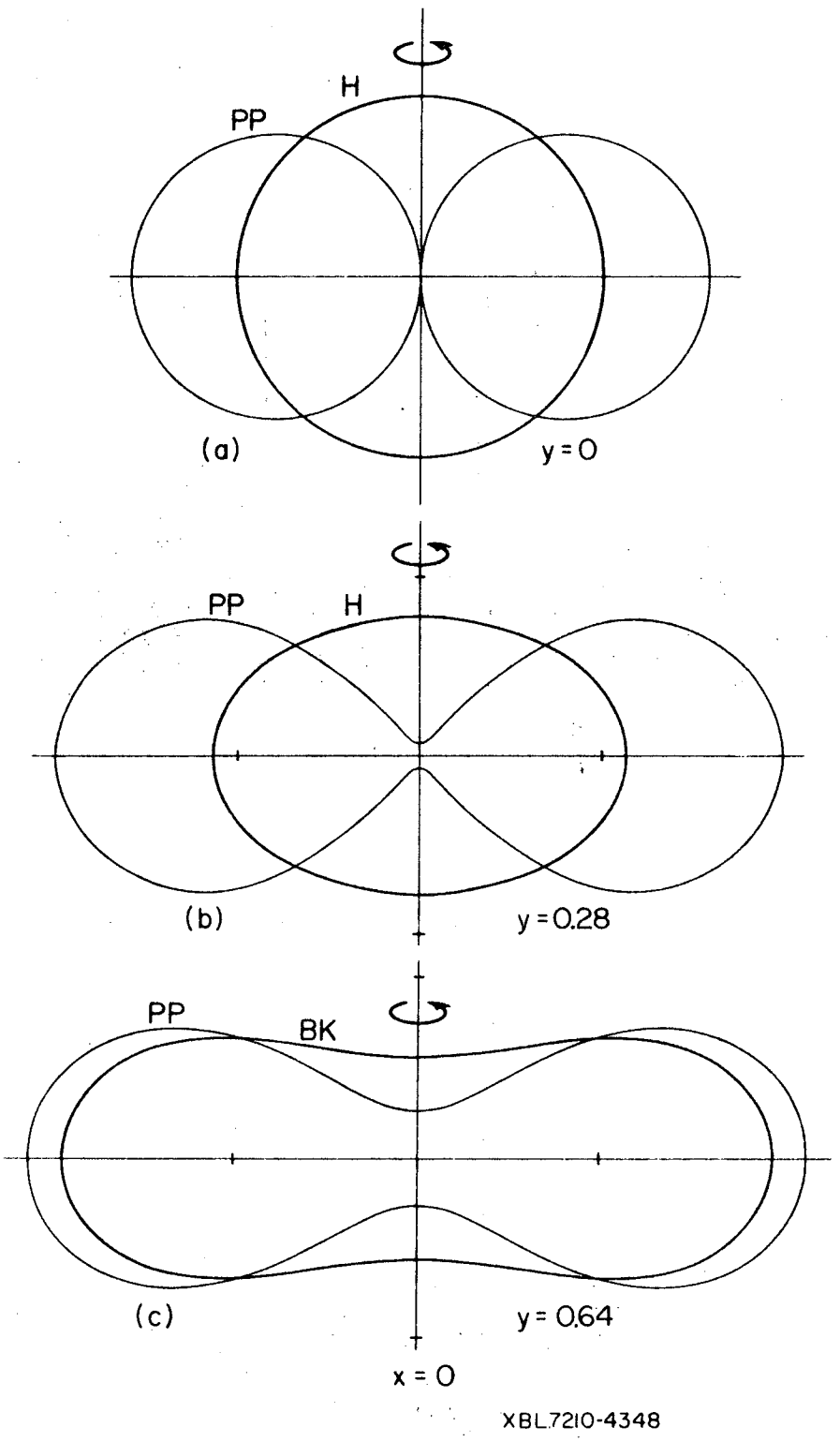

Fig. 4

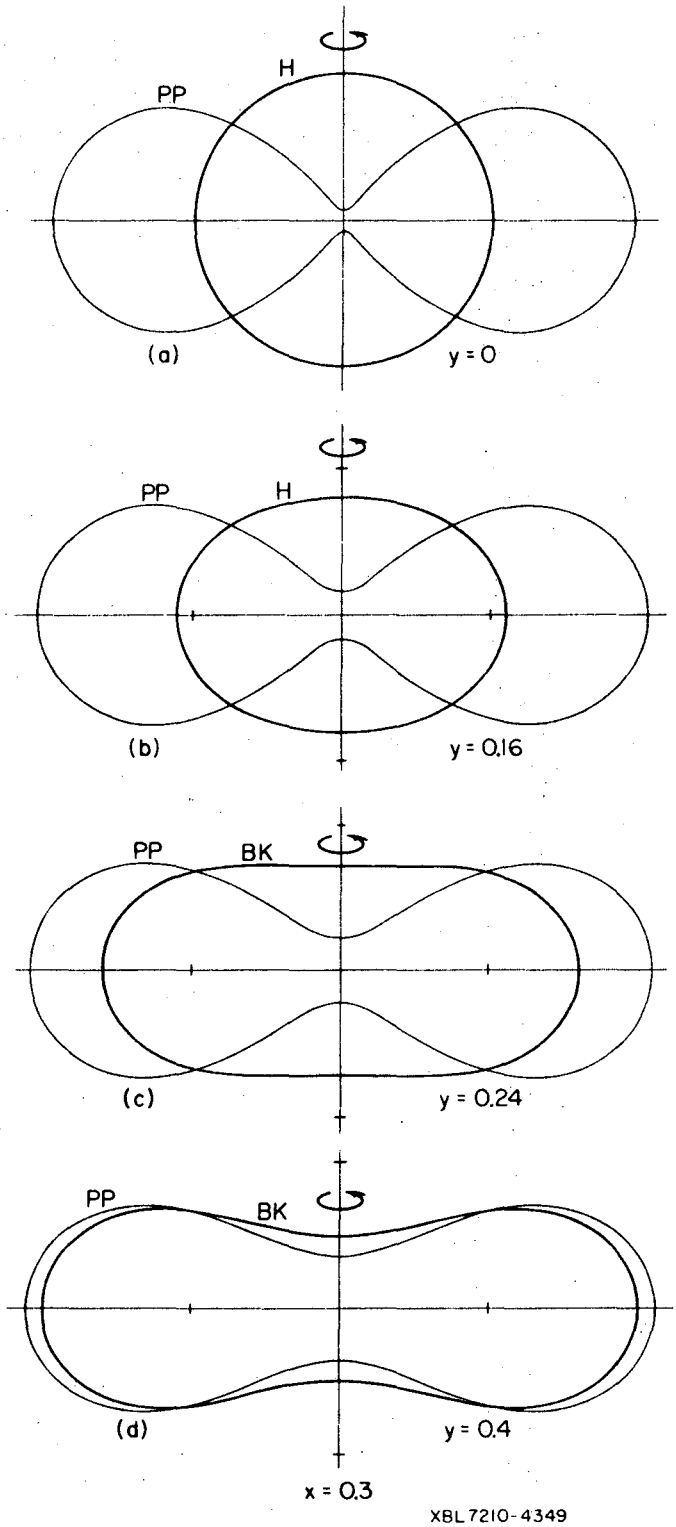

Fig. 5

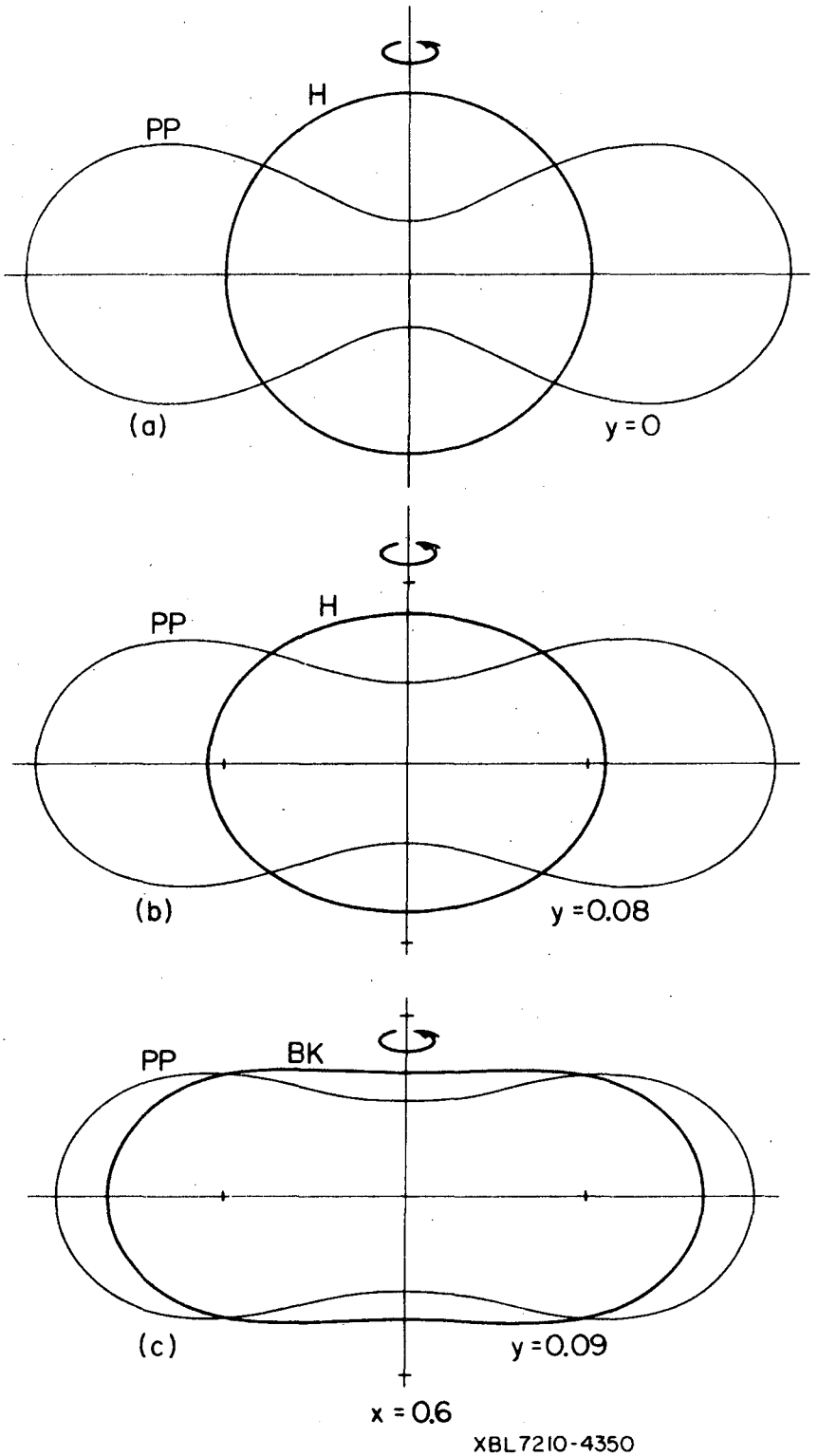

Fig. 6

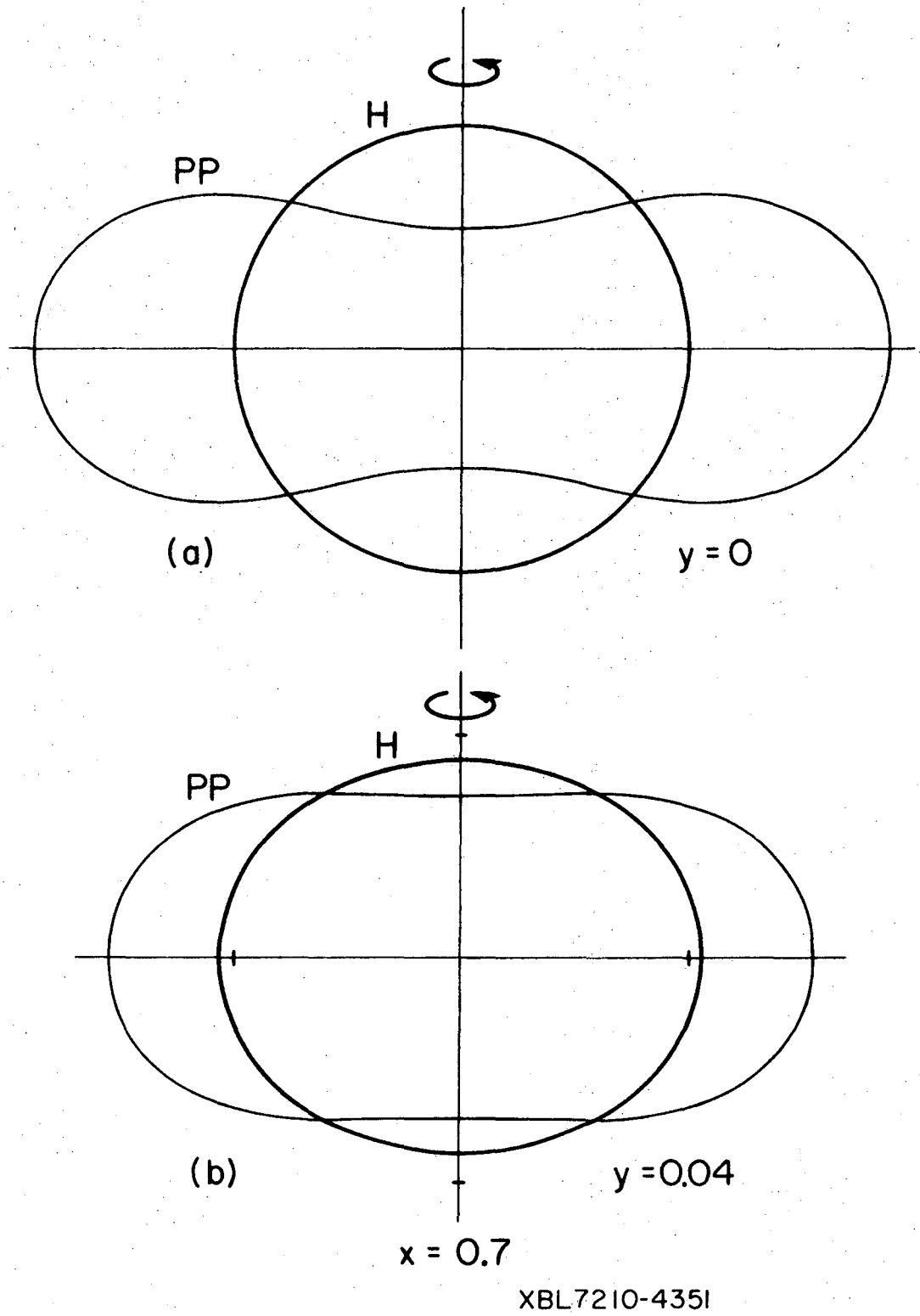

Fig. 7

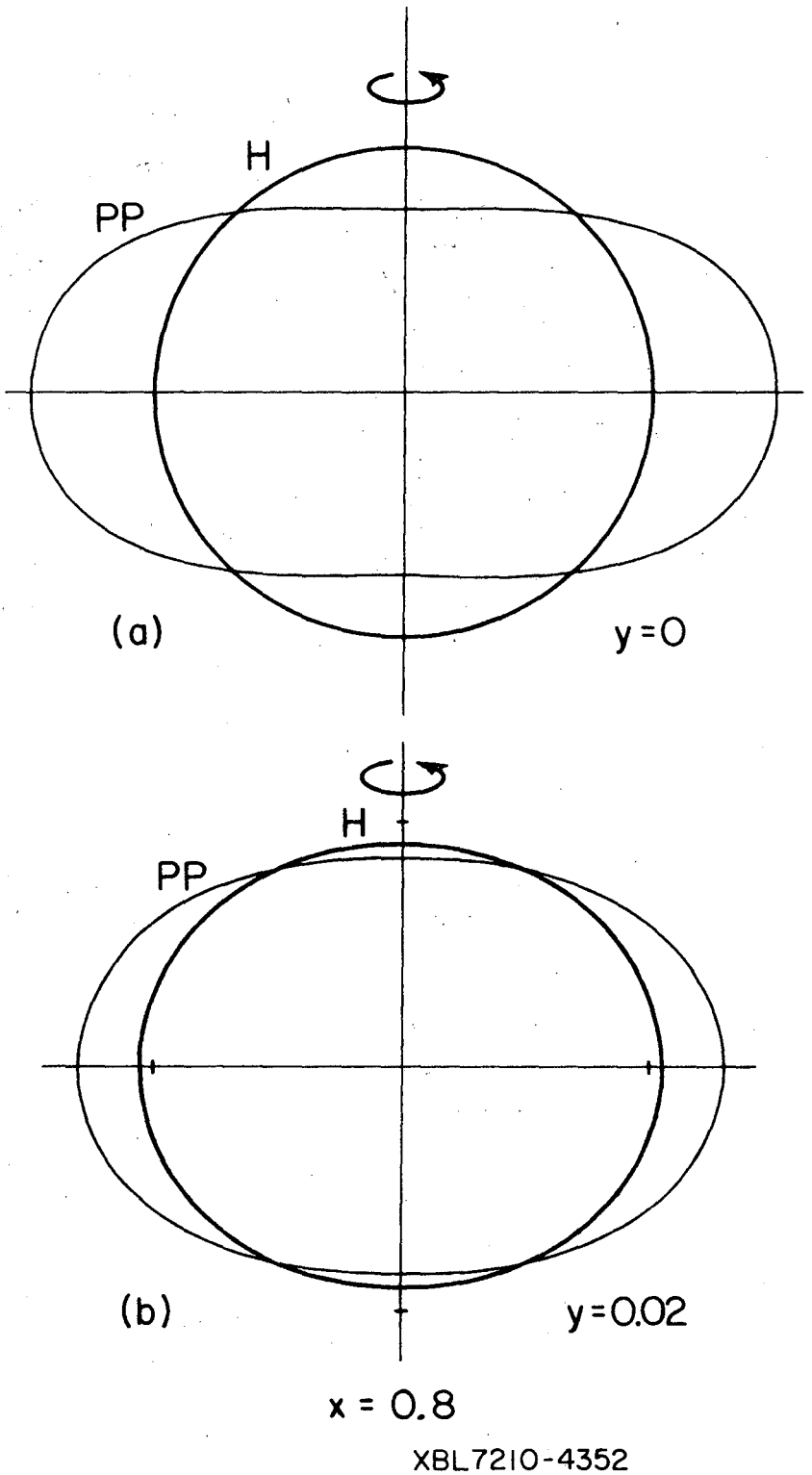

Fig. 8

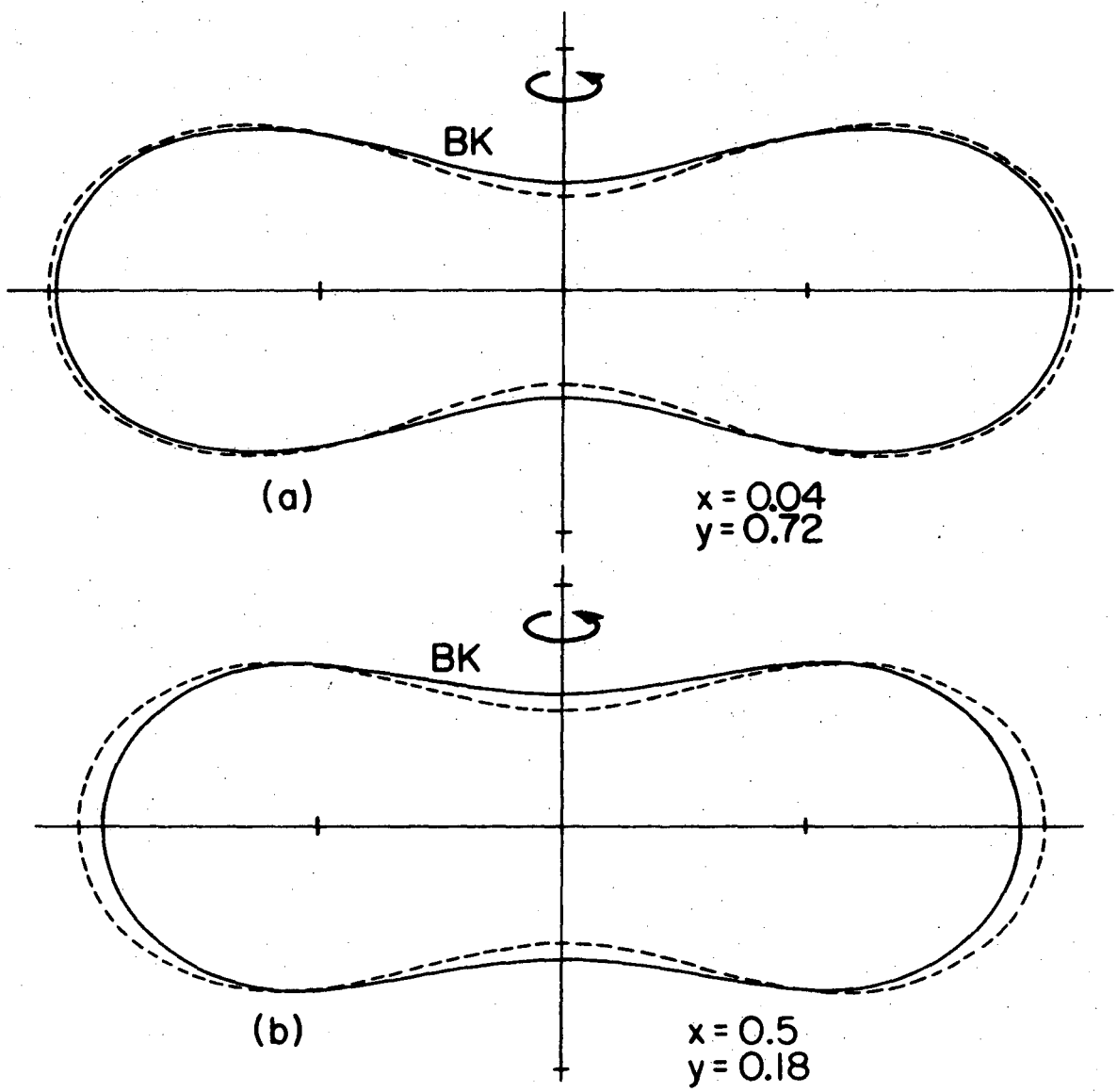

XBL7210-4353

Fig. 9

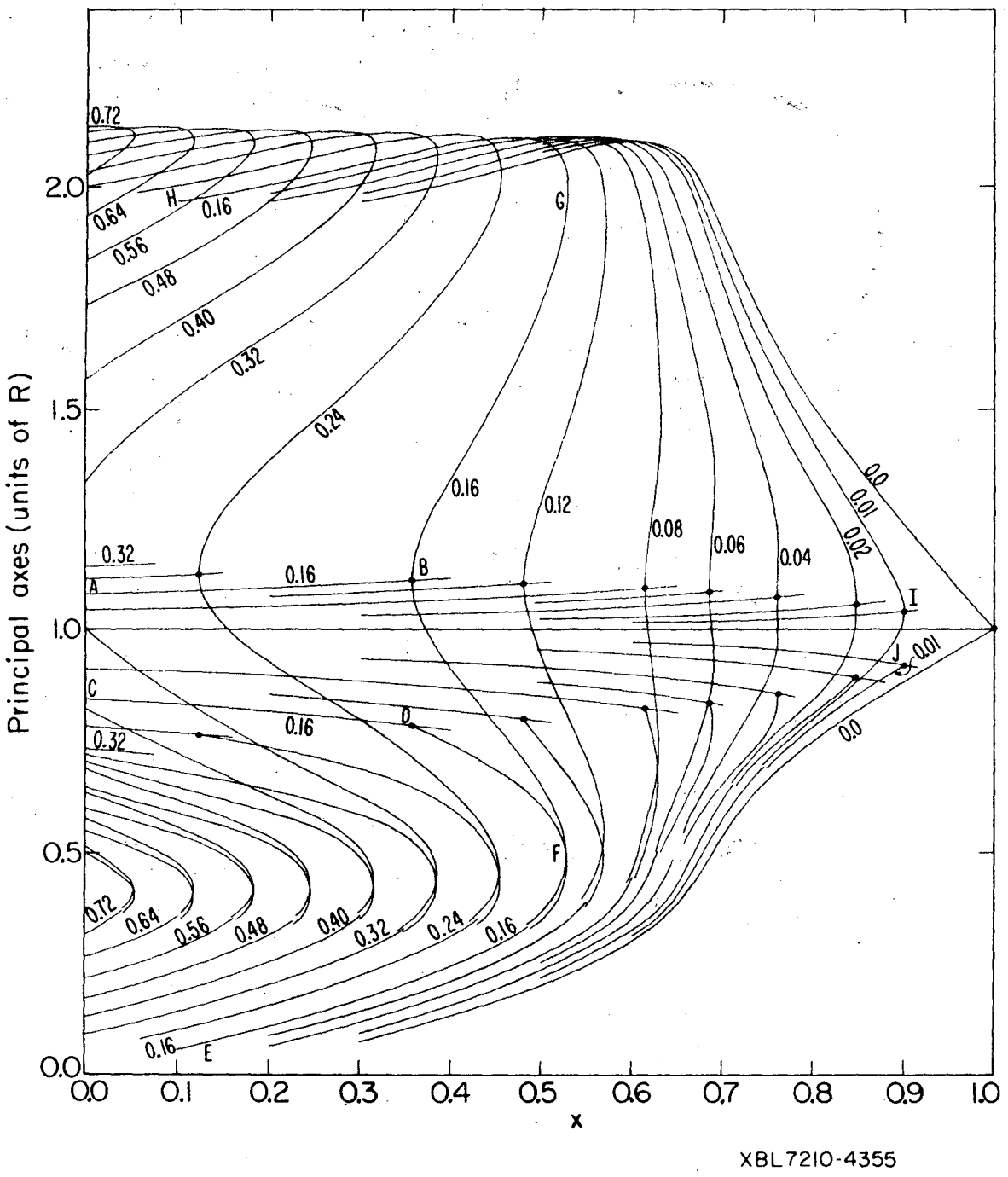
Principal axes (units of R)
x
0.0
0.5
1.0
1.5
2.0
0.1
0.2
0.3
0.4
0.5
0.6
0.7
0.8
0.9
1.0
A
B
C
D
E
F
G
H
I
J
0.72
0.64
0.56
0.48
0.40
0.32
0.24
0.16
0.12
0.08
0.06
0.04
0.02
0.01
0.0
XBL7210-4355

Fig. 10

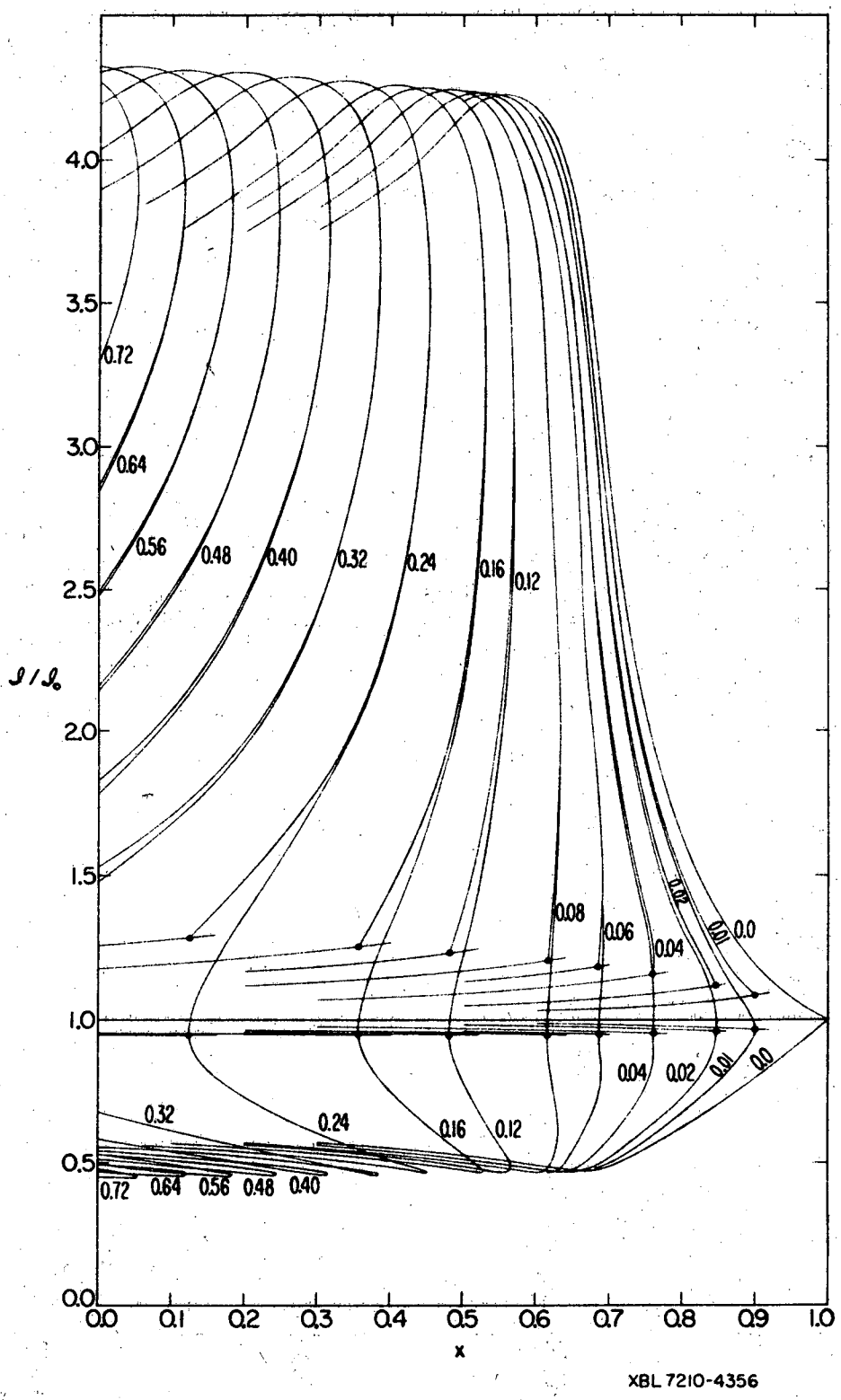

Fig. 11

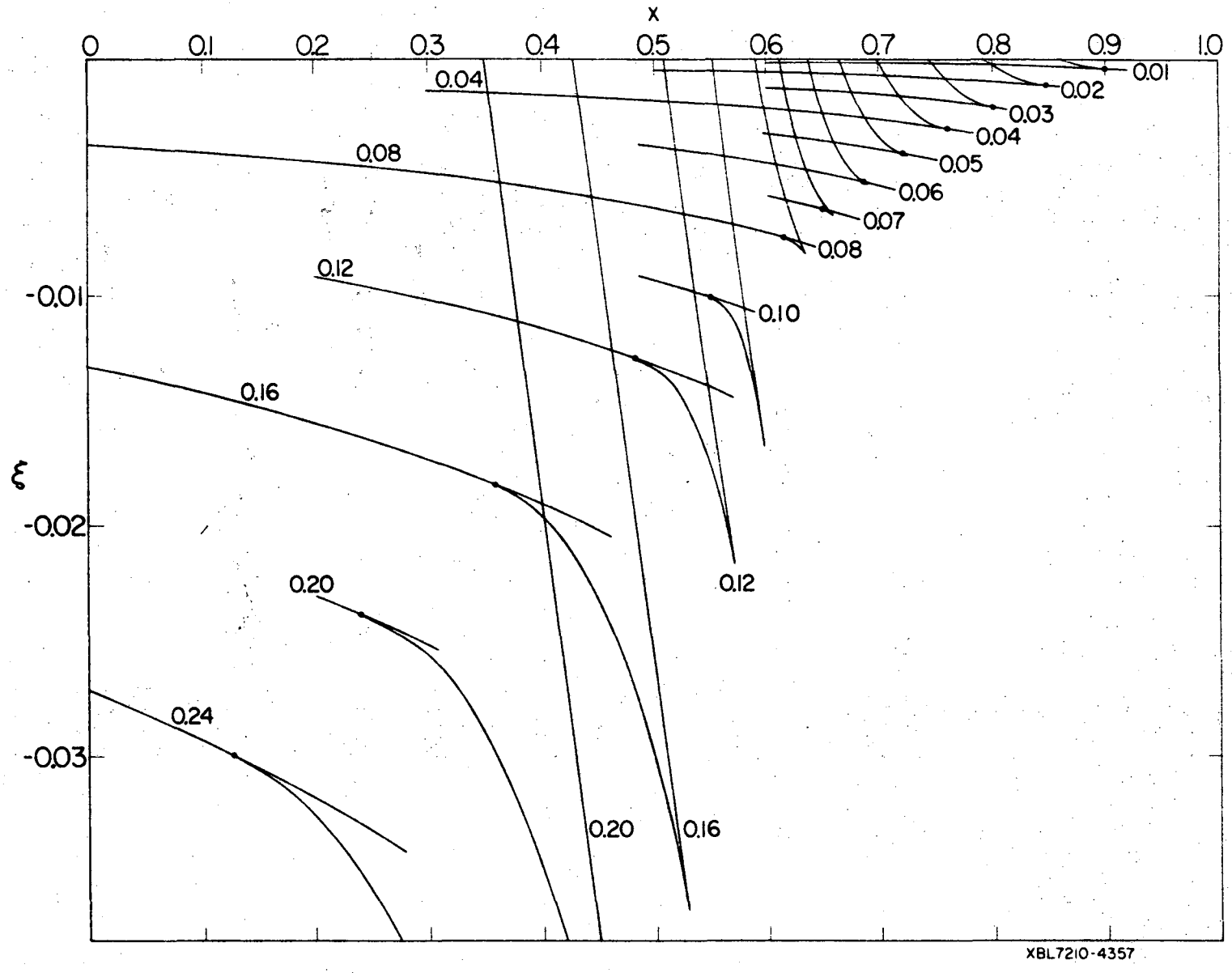
x
0
0.1
0.2
0.3
0.4
0.5
0.6
0.7
0.8
0.9
1.0
ξ
-0.01
-0.02
-0.03
0.04
0.08
0.12
0.16
0.20
0.24
0.01
0.02
0.03
0.04
0.05
0.06
0.07
0.08
0.10
0.12
0.20
0.16
XBL7210-4357

Fig. 12a

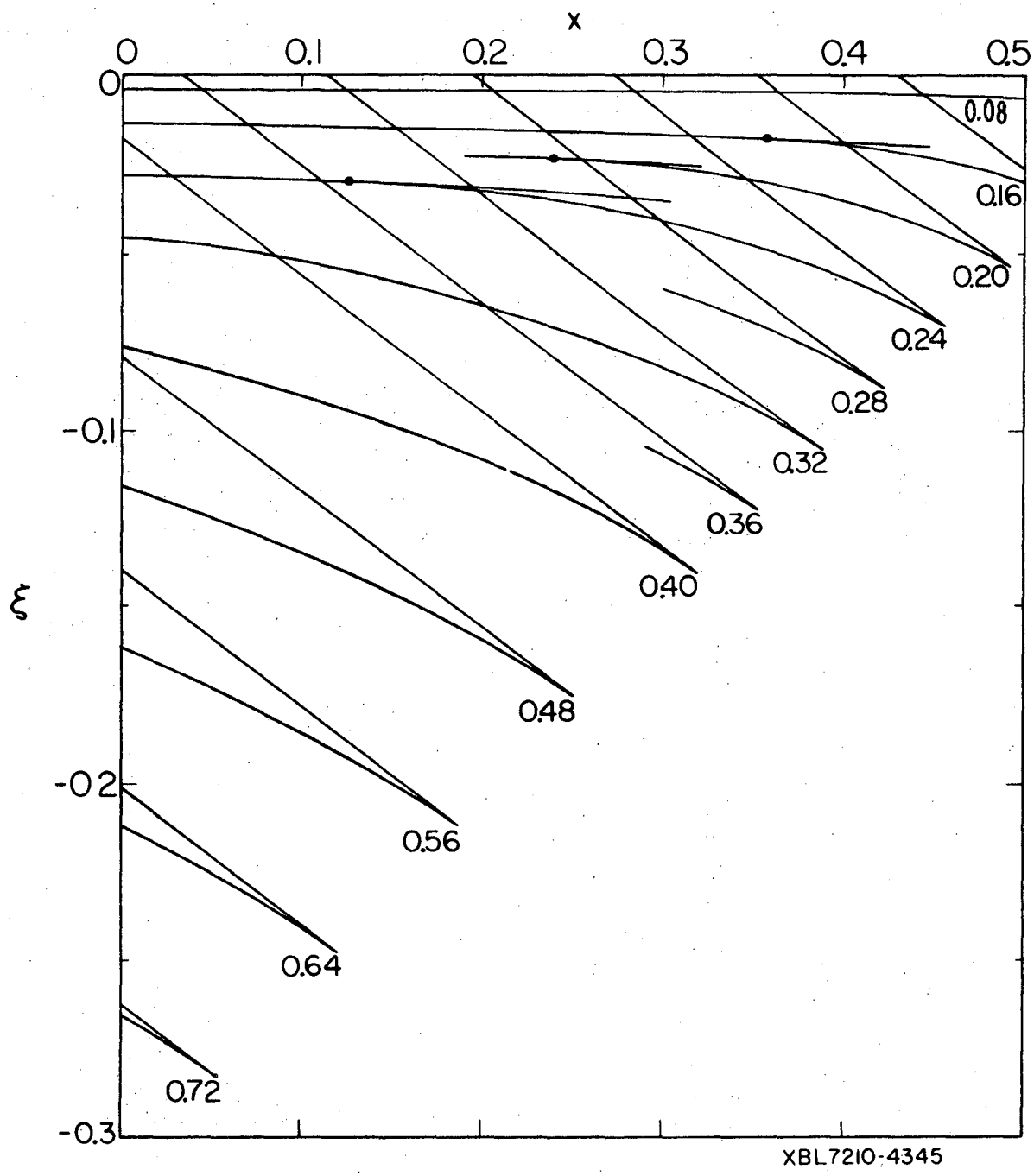

Fig. 12b

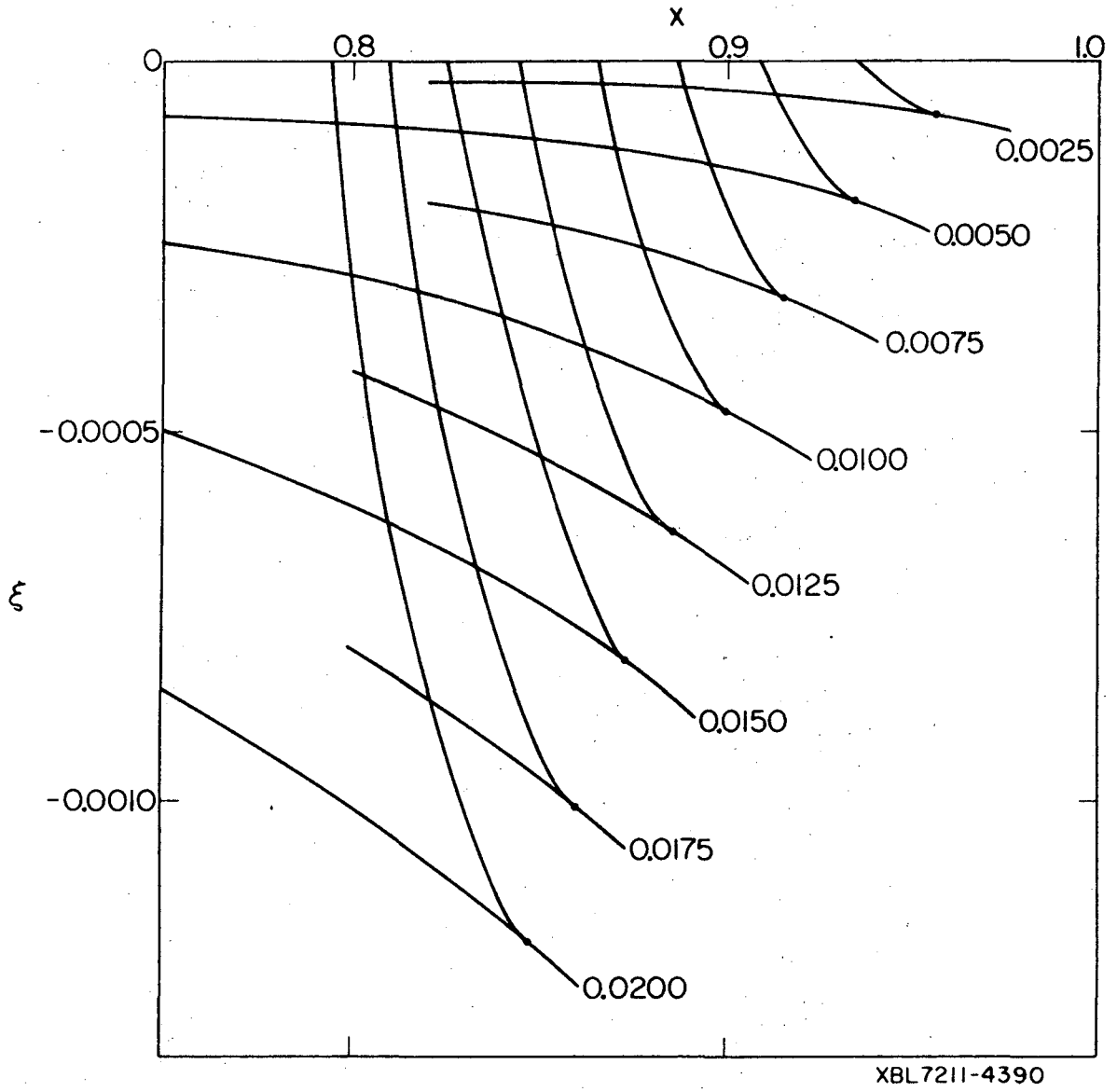
X
0
0.8
0.9
1.0
0.0025
0.0050
0.0075
0.0100
0.0125
0.0150
0.0175
0.0200
-0.0005
-0.0010
ξ
XBL7211-4390

Fig. 12c

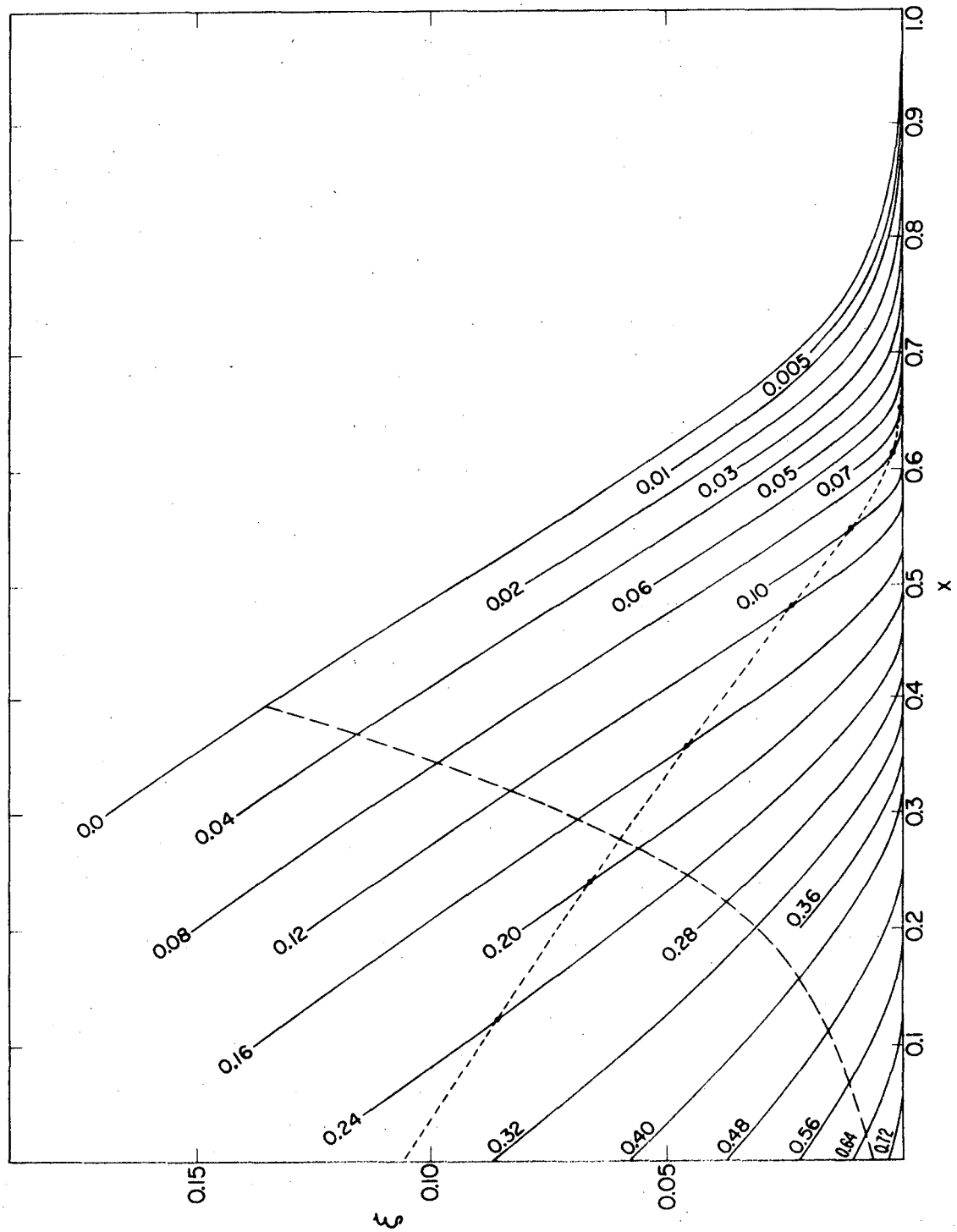
0.005
0.01
0.02
0.03
0.04
0.05
0.06
0.07
0.08
0.10
0.12
0.16
0.20
0.24
0.28
0.32
0.36
0.40
0.48
0.56
0.64
0.72
0.0
1.0
0.9
0.8
0.7
0.6
0.5
0.4
0.3
0.2
0.1
x
0.15
0.10
0.05
ε
XBL 7210-4358

Fig. 13a

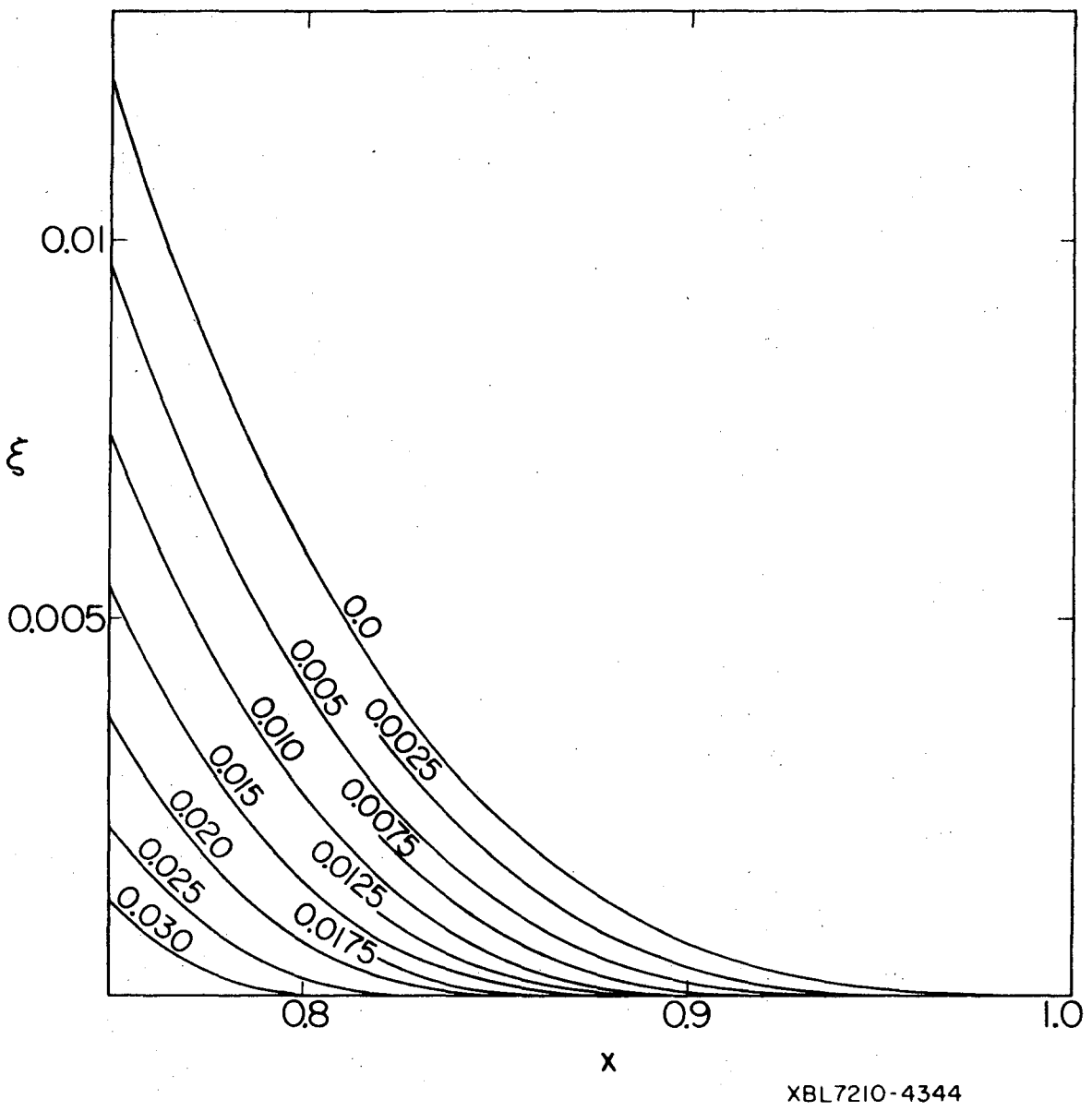
0.01
0.005
ξ
0.0
0.005
0.0025
0.010
0.0075
0.015
0.0125
0.020
0.0175
0.025
0.030
0.8
0.9
1.0
x
XBL7210-4344

Fig. 13b

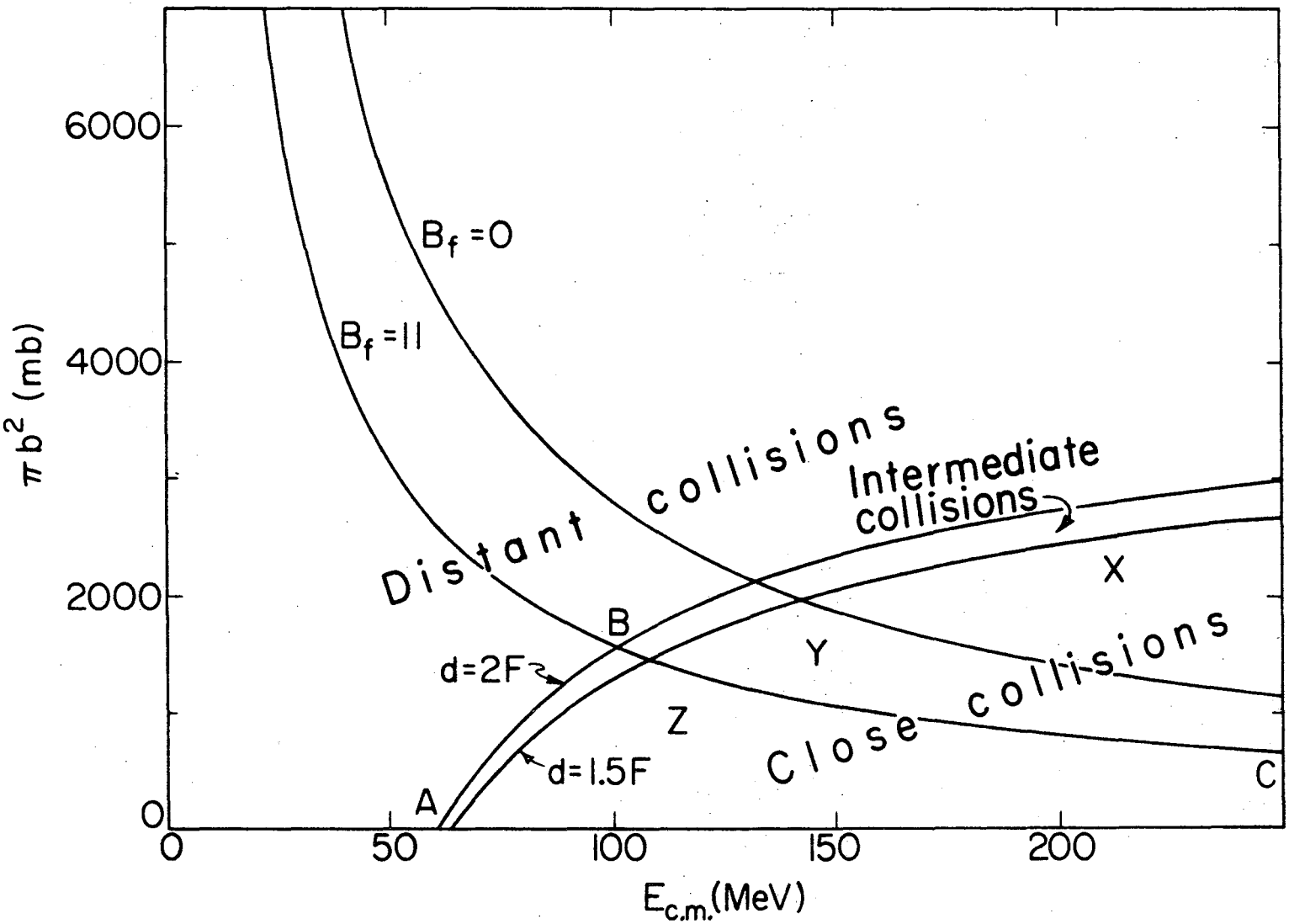

XBL7210-4343

Fig. 14

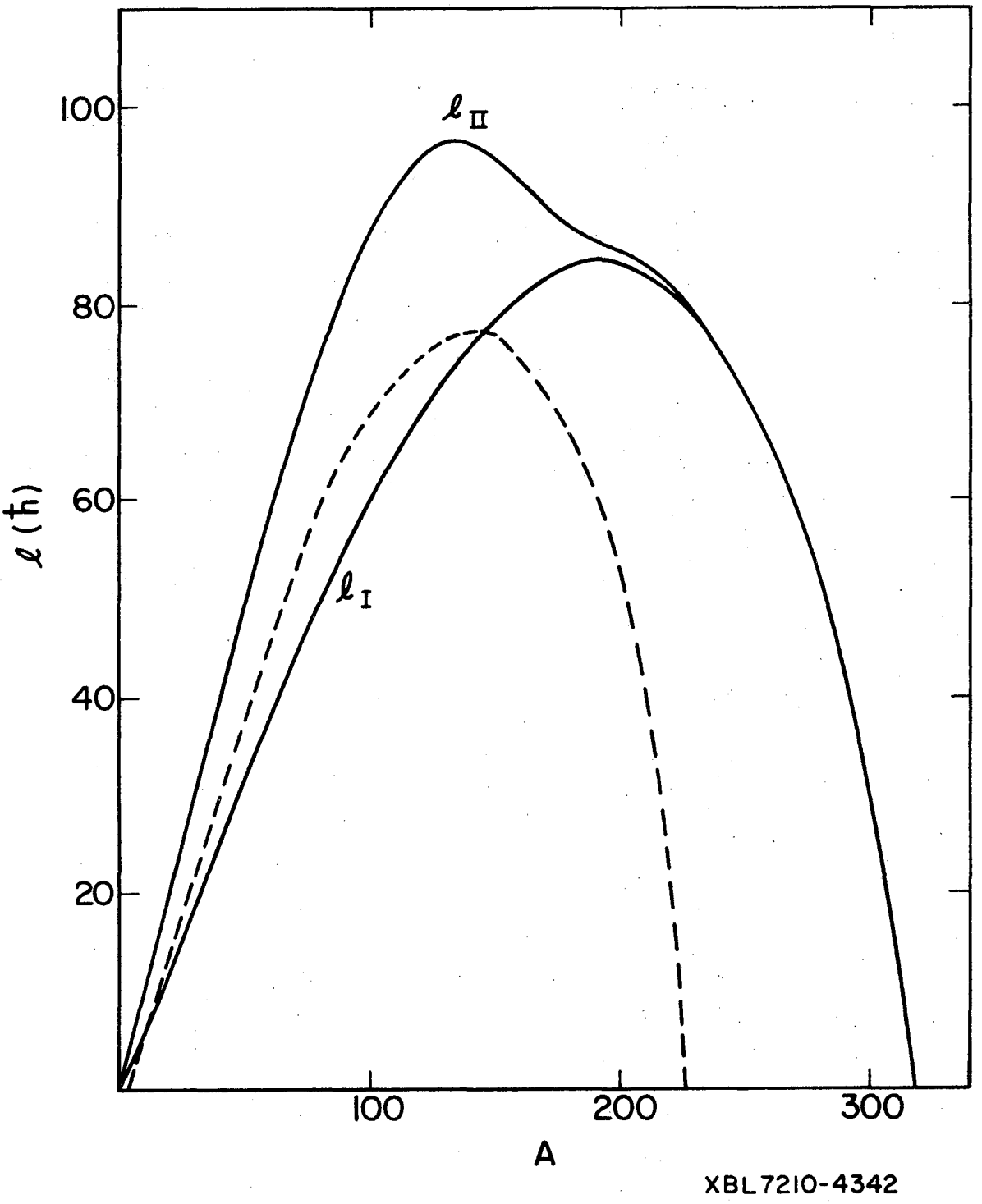

Fig. 15

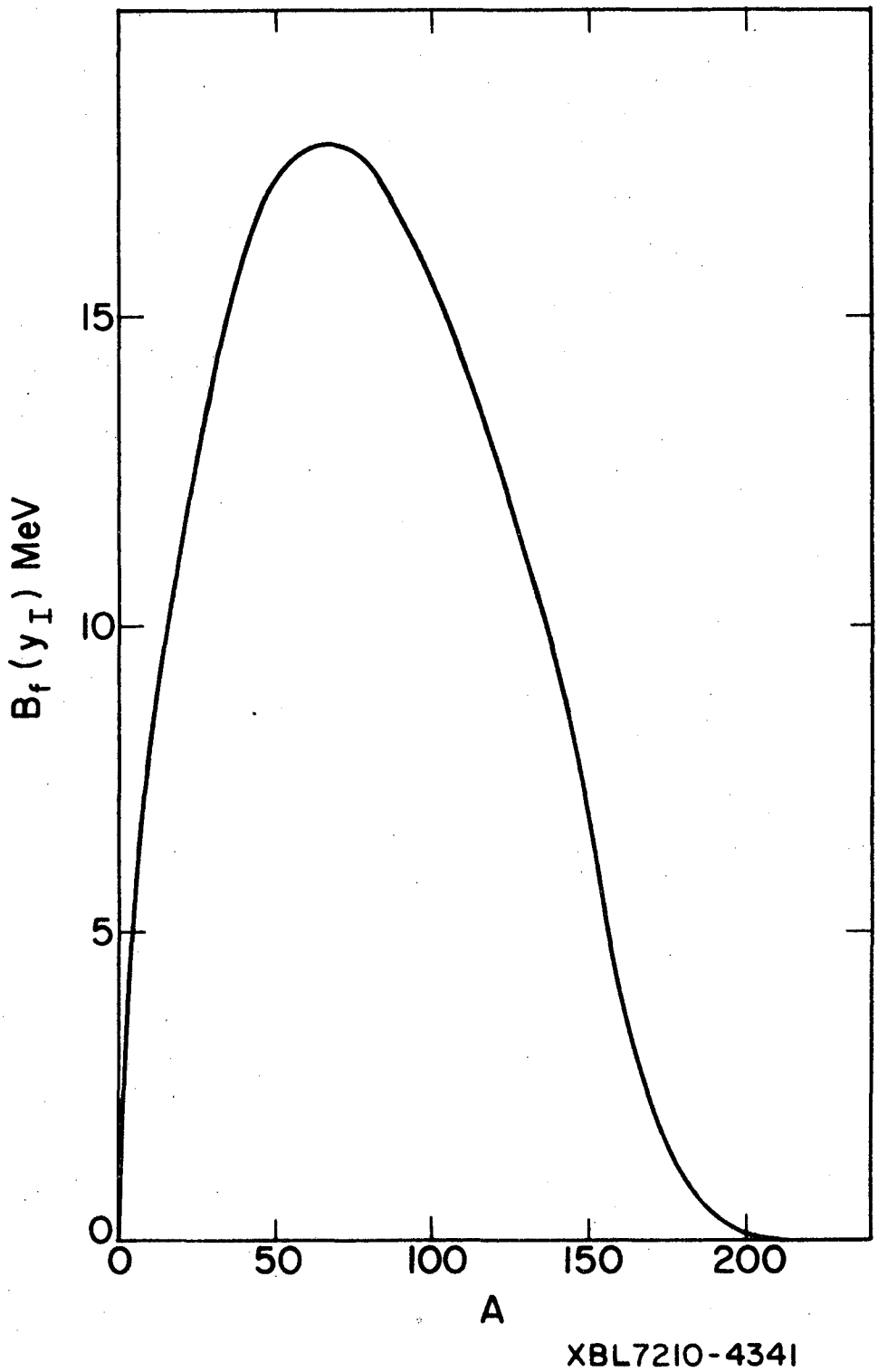

Fig. 16

TECHNICAL INFORMATION DIVISION
LAWRENCE BERKELEY LABORATORY
UNIVERSITY OF CALIFORNIA
BERKELEY, CALIFORNIA 94720